POLITECNICO DI TORINO

I Facoltà di Ingegneria
Corso di Laurea in Ingegneria Energetica e Nucleare

Master of Science Thesis

Energy analysis of two backwash implementations in an ultrafiltration and reverse osmosis PV-powered filtration system

Supervisor:

Prof. Eliodoro Chiavazzo

Prof. Bryce Richards

Candidate:

Michele Milia

December 2019

I assure that I have authored this work myself, that I have completely and accurately stated all the aids I have used, and that I have identified everything that has been taken from work by others unaltered or with modifications.

Torino, the 3. Dezember 2019

Abstract

Water access is a fundamental human right. 300 million people in the sub-saharan region do not have access to clean water. In this area, a PV-powered ultra-filtration (UF) and reverse osmosis (RO) filtration system represents a valid technology to provide drinkable water. In this kind of systems, the maintenance of the membrane is a key factor in order to avoid its obstruction over time (fouling), with a consequent increase in energy consumption; therefore, the choice of a suitable cleaning mechanism and the optimization of its working parameters becomes crucial. With this work, two different backwash cleaning setups have been integrated to an existing PV-powered UF-RO system. The cleaning is performed by the water stored in a bladder tank in the first setup, while in the second configuration the backwash is sourced by a dedicated DC pump. The testing of the two systems has been performed with different cleaning frequencies (from 15 to 120 min), with fixed backwash water consumption (4 L). Bentonite, with a concentration of 500 mg/L, has been chosen as fouling simulation agent and inserted into a feed solution composed by DI water and NaCl (5g/L). Particular interest has been directed to the total specific energy consumption (TSEC) and the UF trans-membrane pressure (TMP) increase due to fouling. The results show that the value of total specific energy consumption (TSEC) plateaus to a minimum value for frequencies longer than 30 min and that the TMP increase is noticeable only for frequencies longer than 45 min. No relevant difference in TSEC or TMP increase has been highlighted, shifting the choice of the suitable cleaning technology to factors like cost and sturdiness.

Ringraziamenti

Vorrei ringraziare il professore Eliodoro Chiavazzo, il professore Bryce Richards, Sheying Li e Ana per questa opportunitá e per l'aiuto ricevuto in questo ultimo semestre.
Non ci sono parole adatte per esprimere tutto il mio affetto e gratitudine per le persone che mi sono state vicine in questi anni, tuttavia abbozzeró un tentativo.
Vorrei ringraziare i miei genitori, Tati e Caló, a cui devo tutto, per essere sempre stati al mio fianco, insegnandomi, in totale libertá, cosa importi veramente nella vita.
Grazie all'infinito amore, pazienza e gioia di Elena, mia compagna di vita; purtroppo per te ci aspettano ancora mille avventure.
La mia gratitudive va anche a Maggie, Eliza, Nat e Emily per avermi accolto come una seconda famiglia.
Grazie Luca e Eli per tutti i momenti passati insieme e per essere diventati i miei modelli di vita.
Vorrei ringraziare tutti i miei amici della ridente Alessandria, in particolare Alessia e i Bombers united.
Grazie a Manu e Noemi, Alessandro, Salvo, Diego, Luca, Alessio, Matteo, Nicola e a tutto il gruppo di Alles Klar per aver reso l'erasmus un'esperienza polemicamente meravigliosa.
Grazie ai miei compagni di mille disavventure universitarie e non, Ciro, Gianluca, Jack, Mao, Andrea e Edo.
Vorrei ringraziare Ario e Hunter per aver dimostrato che l'amicizia supera le distanze.
Infine, un ringraziamento speciale a Gina la guerriera.

Acknowledgements

I would like to thank Professor Eliodoro Chiavazzo, Professor Bryce Richards, Sheying Li and Ana for this opportunity and for the help received in this last semester.
There are no suitable words to express all my love and gratitude for the people who have been close to me in these years, however I will try.
I would like to thank my parents, Tati and Caló, to whom I owe everything, for always having been by my side, teaching me, in total freedom, what really matters in life.
Thanks to the infinite love, patience and joy of Elena, my life partner; unfortunately for you there are still a thousand adventures waiting for us. My gratitude also goes to Maggie, Eliza, Nat and Emily for welcoming me as a second family.
Thanks to Luca and Eli for all the moments spent together and for becoming my life models.
I would like to thank all my friends from the sunny Alessandria, in particular Alessia and the Bombers united.
Thanks to Manu and Noemi, Alessandro, Salvo, Diego, Luca, Alessio, Matteo, Nicola and all the Alles Klar group for making Erasmus a polemically wonderful experience.
Thanks to my mates of many disadventures, Ciro, Gianluca, Mao, Jack, Andrea and Edo.
I would like to thank Ario and Hunter for showing that friendship exceeds distances.
Finally, a special thanks to Gina the warrior.

Contents

Chapter 1

Introduction and motivations

Although being a fundamental human need, clean water access is not guaranteed in many parts of the planet. Water stress is defined as: "the ability, or lack thereof, to meet human and ecological demand for fresh water" [1] and it is a very relevant issue concerning particularly the sub-Saharan area. The estimated number of people suffering from water stress in this area is around 300 million [2], corresponding to one fourth of the total population of the continent. Fig. 1.1 shows the world water availability condition, highlighting that the cause of the African water scarcity is to be found in the economic restrictions of the area, which translates in lack of the proper infrastructure needed for the guarantee of this resource.

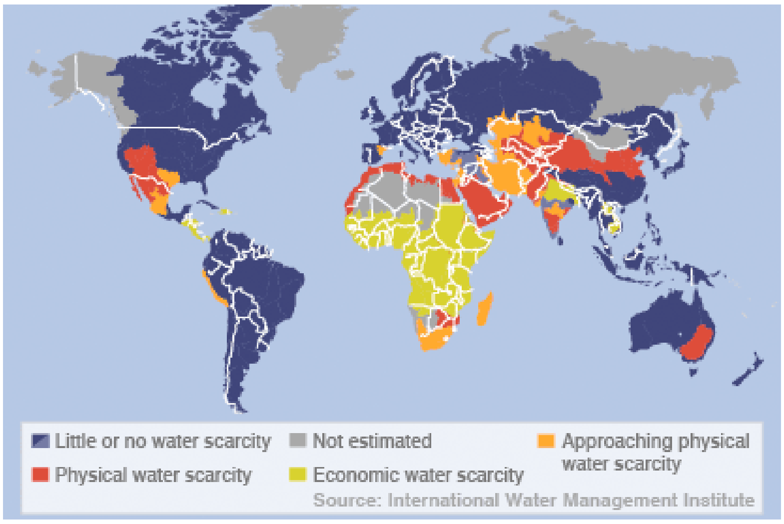

Figure 1.1: Global water accessibility [3].

One of the most promising technologies which could contribute to the solution of this issue is represented by water filtration; in particular, a PV-powered UF-RO membrane filtration system has shown promising results in real field application in Tanzania [4]. The potential of this kind of system is to be found in three important characteristics of the sub-Saharan region:

- The access to electricity is still not spread through the area [5] (Fig. 1.2);
- The risk of contaminated ground water is dramatically high [6] (1.3);
- The solar irradiance offers a relevant amount of available solar energy (Fig.1.4).

Therefore, this system offers the chance to build an off-grid solar powered module that is able to filtrate contaminated ground water, removing salt, organic and inorganic compounds. With this approach, the needs of the area are addressed with its natural energy resources.

One of the challenges of this application is the accumulation of material on the UF membrane surface, the so called fouling, which leads to an increase in energy consumption and to frequent maintenance.

The goal of this work is to integrate to a PV-powered UF-RO membrane filtration system, on both the hardware and software side, two different membrane cleaning options; these will be tested with different operating parameters in order to find the optimal values in terms of energy consumption. A comparison between the two technologies will be finally performed in order to gather the means to chose the optimal cleaning method for a possible real outdoor integration.

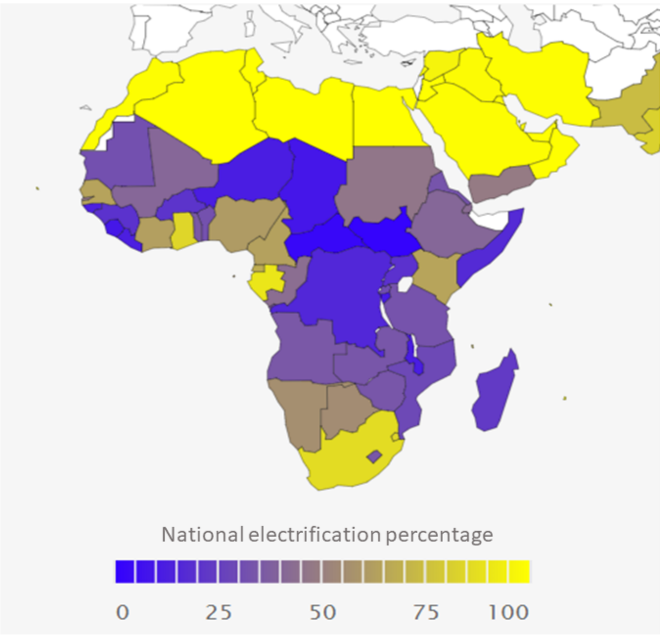

Figure 1.2: National Electrification percentage as published by IEA [5].

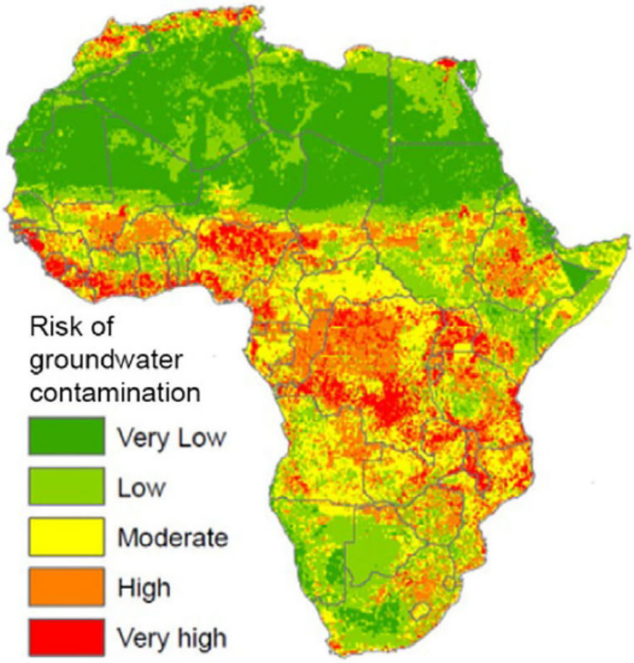

Figure 1.3: African ground water contamination as illustrated by [4] [6].

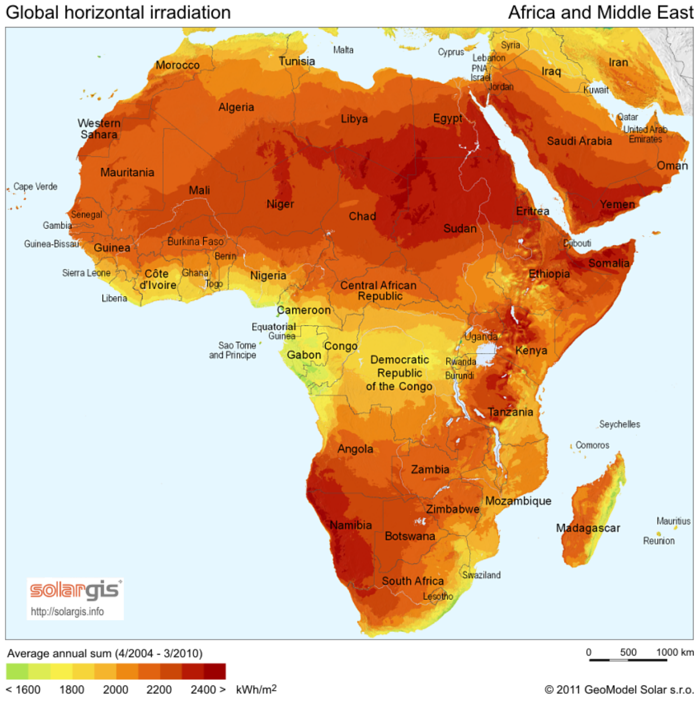

Figure 1.4: Global horizontal irradiation in Africa [7].

Chapter 2

Membrane Fouling and cleaning theory

The goal of the following chapter is to give a theory introduction on the main fouling mechanisms and to the possible solutions. Some practical aspects about membrane filtration application will be given, along with some theoretical knowledge about governing equations and energy consumption. Finally, in order to relate the introduction to real case applications, a brief summary of the most used backwash parameters will be shown.

2.1 Introduction to Membranes

In this section, an overview on the different types of membrane and to possible advantages and disadvantages is given in order to get more familiar with the type of application that will be studied in this work.

2.1.1 Potential and Drawbacks

Comparing to other technologies, membranes show many advantages that make them a promising and a rising popularity solution for many applications [8]:

- **No additives required**:
  Generally, the membrane tecnhologies are clean from any additives, which could potentially be pollutants, since they don't rely on phase equilibrium or mechanical separation mechanisms. This absence of additives leads membranes to be considered as an attractive solution concerning environmental issues.
- **Low energy consumption**:
  As said before, membranes do no rely on phase change separation, which is a par-

ticularly energy hungry mechanism. Therefore their usage is especially suitable for specific application which do not have a constant and abundant energy supply (i.e. renewable energies) or where the energy cost plays a big role in the overall production management choices.

- **Simple setup**:
  Membrane setups have usually a modular nature and do not require much auxiliary equipment. This characteristic makes them easy to install and to use, while determining both the investment and operational costs to increase linearly with the size of the plant. Therefore membrane setups are generally more suitable for little scale production since the upfront investment and management costs are low, while the economy of scale makes other technologies preferable for mass scale production.

Along with many important advantages, this technology presents also some relevant limitations [8]:

- **Flux and selectivity correlation**:
  In membranes application, generally, flux and selectivity are related by an inverse proportionality. This represents a potential problem for mass production, since, often, high permeation is followed by scarce selectivity. A field not negatively affected by this reverse proportionality is the pharmaceutical industry, where high selectivity is far more relevant than quantity production.
- **Dependability**:
  Scaling up of membrane processes has often dependability issues; indeed, membrane setups are extremely related to the specific applications they are built for, depending on feed material and desired permeate. This aspect doesn't allow an easy and universal scaling up of such plants, since specific preliminary tests are generally required for a correct technology application.
- **Sensitivity**:
  One of the main problems, especially concerning polimeric membranes is their intrinsic instability. One of the main drawbacks of this aspect is the membrane fouling, which significantly decreases the setup performance and that imposes a limit to the range of possible membrane application fields.

2.1.2 Membrane classification

Membranes have a wide range of composition materials and applications. In general, a relevant classification is given by the different membrane driving mechanisms [9]:

- **Pressure**:
  An imposed pressure gradient is able to separate pollutants or in general undesired particles from the solution. This type of membrane is further classified as shown in Fig. (2.1) in microfiltration (MF), ultrafiltration (UF), nanofiltration (NF) and reverse osmisis (RO).

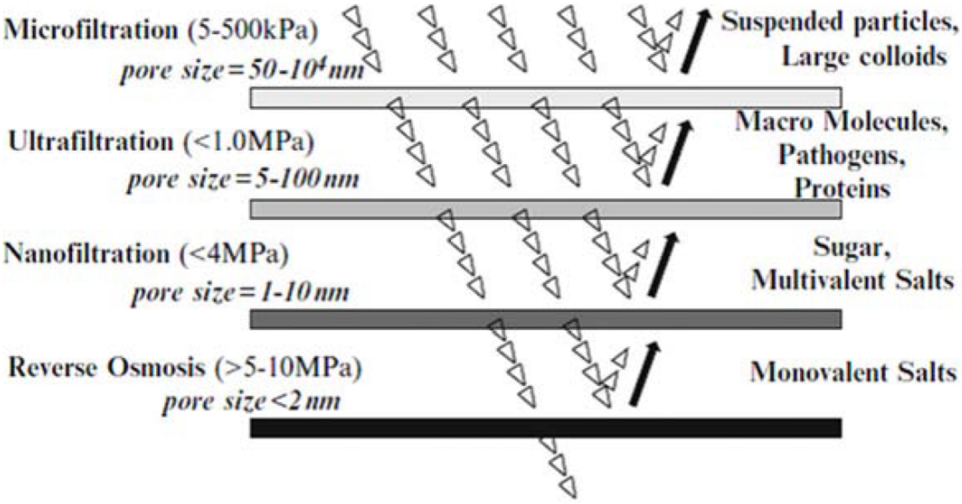

Figure 2.1: Different pore size membrane classification and corresponding material removal as shown by [10].

- **Solute transfer**:
  In this case the driving source that cause a separation between solute and solution could be either electrochemical (ED), diffusive (D) or the preferential solubility effects (LM).

- **Heat**:
  The liquid feed solution is heated so that it faces a phase change permeating the membrane. Examples are membrane distillation (MD) and pervaporation (PV).

- **Hybrid**:
  Multiple configuration are possible matching the membrane unit with a different unit process like adsorption, ion exchange or coagulation.

2.2 Nature of flux decline

After the introduction on the working principles of membranes, in this section the reasons behind permeability loss will be analyzed. As described by [11] there are two main causes for the membrane flux decline: concentration polarization and fouling. In the following section the two mechanisms will be described, with a special focus on fouling, due to its relevance in this work; in particular the different fouling modes and the solute particles involved in the phenomena will be overviewed.

2.2.1 Concentration polarization

Due to the intrinsic selectivity of the membranes the solution particles that do not permeate the membrane are accumulated in a layer close to the membrane surface. Since the back diffusion rate to the solution of such particles is slower than the accumulation rate on the surface layer, a concentration gradient is formed; indeed the surface concentration could reach up to 50 times the one in the original solution [12]. Even if the process is considered reversible, an osmotic backpressure is created in correspondence of such boundary layer, leading to an overall membrane TMP reduction (as it will be further studied in section 2.3).

2.2.2 Fouling

The second main phenomenon that causes a flux decline is fouling. Due to its complexity, the influence of the different types of interactions between the various fouling agents on the obstruction of the membrane is very difficult to accurately predict. In general, it is possible to group the results of these interactions into four different categories, as it is well explained by [11]: in-pore adsorption, pore blockage, cake formation, and finally gel formation, as it is illustrated in Fig. 2.2.

Adsorption

Accordingly to the review work of [11], adsorption is due to attraction forces acting between the foulant and the membrane. The three main phenomena responsible for this kind of fouling are: weak Van Der Waals forces, chemical bonding and electrostatic attraction. The thermodynamics of the system, along with the bonding energy above cited, make the adsorption very hard to remove with physical cleaning, requiring in many instances chemical washing.

In-pore Adsorption or In-pore Deposition

When the size of the foulant particle is smaller than the filtration pores, the membrane is susceptible to the in-pore adsorption or deposition, depending on the forces equilibrium between membrane and particle . As a result, the overall resistance of the membrane is increase due to a reduction of the pore channels [13].

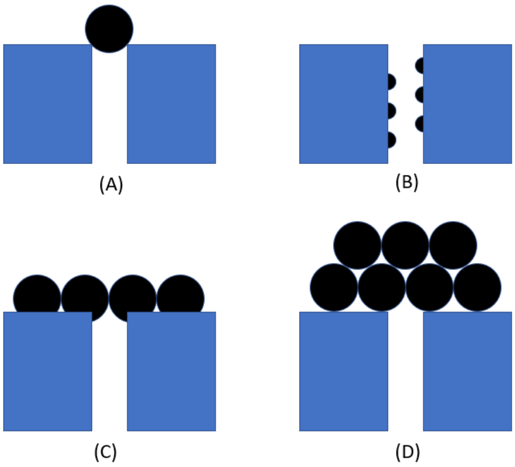

Figure 2.2: Different membrane fouling modes (modified after [13]): (A) Pore blockage, (B) In-pore Adsorption, (C) Adsorption, (D) Cake formation.

Pore blockage

Pore blockage is typical of the first stage of filtration and it regards the particle that have a size comparable with the one of the pores. The filtration channel is completely sealed directly by the particle or through the formation of fouling bridges. In many applications in which the filtration flux is kept constant, the reduction of the number of available pores leads to an increase in the local flux, determining a potential collateral increase of the other fouling mechanisms [11].

Cake formation

Finally, the fouling cake is formed by the different particles that do not enter nor seal the channels. These form layers that accumulate over time on the membrane surface. This cake increases the overall membrane resistance and on one hand, could be seen as a "filter-aid" [14], since it would prevent the highly fouling particles to be in contact with the membrane surface, while on the other hand it could cause a bridge effect which would increase the membrane fouling rate [15].

2.2.3 Foulants

The amount of potential membrane applications imposes a wide variety of possible materials that could interact with the membrane surface and therefore material deterioration or fouling. In general, the particles involved in the most common filtration processes are possible to divide in the following categories [16]:

- **Particulates**:
  The particles not deformable, having a diameter ranging from $1nm$ to $1\mu m$, are considered as colloidal particulates [11]. Basing on their size they can determine the in-pore blocking of the membrane or the cake formation on the surface, the latter being in most cases the dominant effect with filtration time.

- **Macromolecules**:
  The macromolecules category comprehends a wide variety of foulants.
  Proteins are part of this group and they represent one of the main problems regarding irreversible membrane fouling, particularly in the pharmaceutical industry [11]. Indeed, the intrinsic instability of the protein molecules leads to a strong bonding potential with the membrane surface, causing a degradation of the filtration parameters [17].
  Natural organic matter (NOM) also falls into this category, comprehending among others allochtonous and autochtonous organic matter, along with waste mater effluent organic matter (EFOM) [11]. The study of the fouling due to these macromolecules is very relevant since it is one of the main fouling agent in water treatment. Indeed up to 80% of the total organic carbon in natural water is made of NOM (in particular, Humic substances) [18].

- **Ions**:
  Ions, in particular metal ions, could lead to a scaling coagulation layer on the membrane surface. This layer could create material bridges which could accelerate the fouling process [11]. Furthermore the ions charge could lead to the screening of the repulsive forces between the surface and the foulants, increasing the membrane surface adsorption process and therefore fouling.

- **Biological Substances**:
  Active organisms can attach to the membrane surface and form the so called conditioning film, which can grow with time, taking advantage of the nutrients brought by the feed flow in water filtration applications. This kind of foulant is extremely hard to control since the composition of the conditioning film is strongly depending on the feed fluid and it could critically influence the permeation performance of the application due to the additional membrane resistance of the biofilm.

2.3 Introduction to fouling governing equations

After having described the causes of membrane fouling in the previous section, the goal of this chapter is to relate these phenomena to their reference governing equations. First, in order to clearly and easily describe the effects of membrane fouling on permeation parameters, in particular regarding the permeation flux, a simplified permeation model without colloidal particles will be proposed. Then, in the following part, a further grade of complexity will be added, with the introduction of a foulant agent.

2.3.1 Permeation with no fouling

As effectively described by [13], in general, Darcy's law is fitted for describing the flux through a membrane that has as a driving parameter the difference in pressure between the feed and the permeate side:

$$J = P * (p_f - p_p) = P * \Delta p \tag{2.1}$$

With J referring to the volumetric flux, Δp to the pressure difference (or TMP) and P to the permeability constant. The latter is a function of the membrane conformation and can be relatively easily deducted when the structure of the membrane is regular and comparable to well defined shapes. For example the Carman-Kozeny equation is suited for membranes associated to spherical particles packings, while the Hagen-Poiselle equations is preferable for membranes comparable to uniform capillaries.

In order to keep the analysis general, and not restricted to ideal shapes, often far from the not uniform nature of the many commercial membranes, [13] introduces the following equations:

$$J = \frac{\Delta P - \Delta \pi}{\eta R_m} \tag{2.2}$$

$$J = \frac{\Delta P}{\eta (R_m + R_{cp})} \tag{2.3}$$

With equation (2.2) the membrane resistance R_m is introduced.η refers to the dynamic viscosity of the permeate, while $\Delta \pi$ represents the contribution of the concentration polarization and it could be expressed also as resistance R_{cp} as can be seen in equation (2.3).

2.3.2 Permeation with fouling

Fouling flux

Having defined a simple model for describing the flux J in a fouling free scenario, it is now possible to introduce in the previous equations three additional quantities, which represent the different influences of fouling on the overall membrane resistance [13]:

$$J = \frac{\Delta P - \Delta\pi}{\mu(R_m + R_{ads} + R_{rev} + R_{irrev})} \tag{2.4}$$

The equation 2.4 divides in four resistances in series the overall membrane resistance, which is deducted experimentally as a single value: R_m represents as already stated the unfouled membrane resistance, R_{ads} describes the the additional membrane resistance due to the colloidal adsorption on both surface and pore level, R_{rev} and R_{irrev} indicate respectively the reversible and irreversible additional membrane resistance. With this approach the author chooses to not include R_{ads} within the reversible or irreversible resistances since the first is not dependent of the flux, while the latter are strictly correlated to the flux.

Critical flux

As very exhaustively reviewed by [19] the concept of critical flux J_{cs} is not uniquely defined. One of the most suited definitions to our analysis is given by [20], where the critical flux is defined as "a flux below which a decline of flux with time does not occur; above it fouling is observed". In particular, as it can be noticed in Fig. 2.3, the critical flux is distinguished between the "Strong form", where no fouling occurs until the reach of J_{cs}, with a consequent deviation from the pure water line, and the "Weak form", where fouling occurs immediately, but the trend stays linear until it reaches J_{cs}. The two distinctions are made for differentiating between no fouling and fouling conditions respectively.

The analytical representation of the effects of critical flux on the flux equation for the Strong form is given by [19]:

$$For \quad J < J_{cs} : J = \frac{\Delta p}{\mu R_m} \tag{2.5}$$

$$For \quad J > J_{cs} : J = \frac{\Delta p}{\mu(R_m + R_{rev} + R_{irrev})} \tag{2.6}$$

The equation just shown above assume the value of R_{ads} as negligible in flux operating conditions compared to the the other resistances. Furthermore if the effects of concentration polarization needs to be included in the application analysis (i.e. UF membranes), the osmotic effects must be included in analogy with equation 2.4.

Rate of permeability loss, threshold flux concept

The idea of threshold flux has been analysed by [21] in the optics of exploring the concept the "sustainable flux", or rather the flux that corresponds to a good compromise between producing permeate (desired product) and causing the membrane fouling

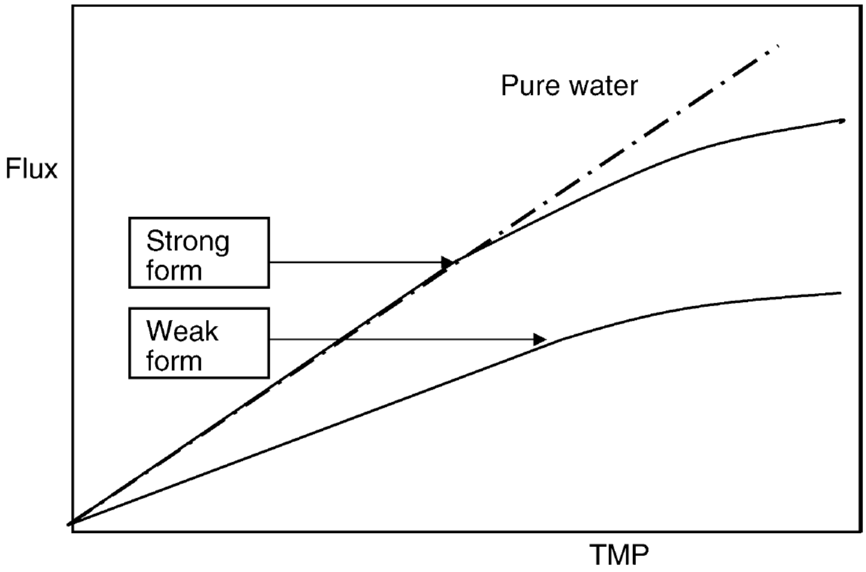

Figure 2.3: Two different forms of critical flux as indicated by [20]

(undesired effect). In particular 4 different waters have been adopted for the filtration experiments ground water, two different surface waters and waste water. The analysis uses TMP as fouling indicator through permeability loss and shows that it is possible to identify a threshold flux J^*, below which the TMP increase presents a linear trend. Proceeding above J^* the membrane fouling increases exponentially.
Therefore it is possible to express the Rate of permeability loss as:

$$For \quad J < J^* : \quad Rate \quad of \quad permeability \quad loss = a \tag{2.7}$$

$$For \quad J > J^* : \quad Rate \quad of \quad permeability \quad loss = a + b(J - J^*) \tag{2.8}$$

Where a and b are empirical constants depending on the membrane system analyzed.

2.3.3 Pore scale approach

Due to the intrinsic complexity of the problem, membrane fouling effects are commonly studied through macro scale experiments, prioritizing the analysis of the consequences of system fouling over the exact causes behind the phenomenon. Even if this approach, which is very useful for large scale real systems, will be described in the following sections, in this chapter a brief overview of the main pore scale fouling analysis will be presented.

DLVO Theory

In order to explain the fouling mechanism at pore scale, a basic introduction to the principal interaction between particle surfaces is required. The main contribution to the the modeling of the particle-particle behaviour is given by the DLVO (Derjaguin, Landau, Vervey and Overbeek) theory [22]. As effectively illustrated by [23], the DLVO theory divides the free energy per unit area between two particles in two main contributions, the Van der Waals and the double layer interactions:

$$W(h) = W_{vdW}(h) + W_{dl}(h) \tag{2.9}$$

In particular the two contributions are defined as:

$$W_{vdW}(h) = -\frac{H}{12\pi h^2} \tag{2.10}$$

$$W_{dl}(h) = \frac{2\sigma_+\sigma_-}{\epsilon_0\epsilon\kappa}\exp\left(-\kappa h\right) \tag{2.11}$$

Where h is the distance between the two surfaces and H represents the Hamaker constant, which is an indicator for the force intensity and it is expressed in Joules. H is often in the range of 10^{-21} and 10^{-19} and with its positive sign makes the VdW force attractive. σ_+ and σ_- represent the surface charge densities per unit area for the two different particles, ϵ represent the dielectric constant of water, while ϵ_0 indicates the permittivity of vacuum. Finally, κ is the symbol for the inverse Debye length.

Simplifying the analysis to the symmetrical case, namely to particles with the same or very similar dimensions, typical of colloidal solutions, it is possible to plot the total force and energy potentials as functions of the distance between the two bodies.
The parameters chosen for Fig. 2.4 are: $H = 5.0 * 10^{-21} J$, $\sigma = 2 \quad mC/m^2$ and a monovalent salt concentration of $8 \quad mM$. In the plot it is possible to distinguish the two different contributions to the total DLVO theory force which depending on the sign is attractive when negative and repulsive when positive. The figure also shows that the attractive vdW forces are more influential at narrow and extended distances, while the double layer is the principal interaction for medium particle separation. The maximum is located at a distance close to the Debye length κ^{-1}, which for water at room temperature can be approximated to:

$$\kappa^{-1} = \frac{0.3 \quad nm}{\sqrt{I}} \tag{2.12}$$

Where I is the ionic strength defined as:

$$I = \frac{1}{2}\sum_i z_i^2 c_i \tag{2.13}$$

With z_i^2 being the valence of the ion of type i, c_i the concentration in mol/L, and i indicating all the different ions present in the solution.

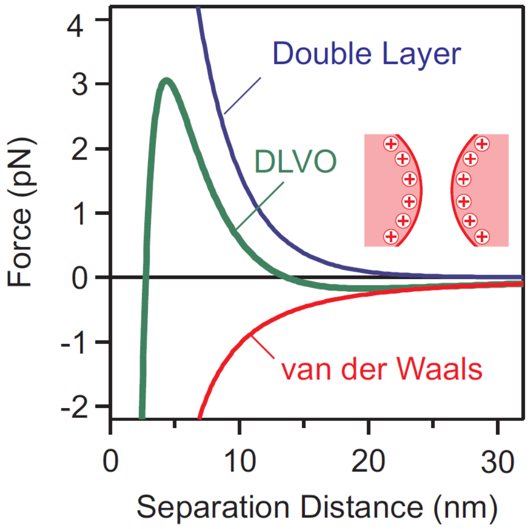

Figure 2.4: Acting force as a function of Separation distance as shown by [23].

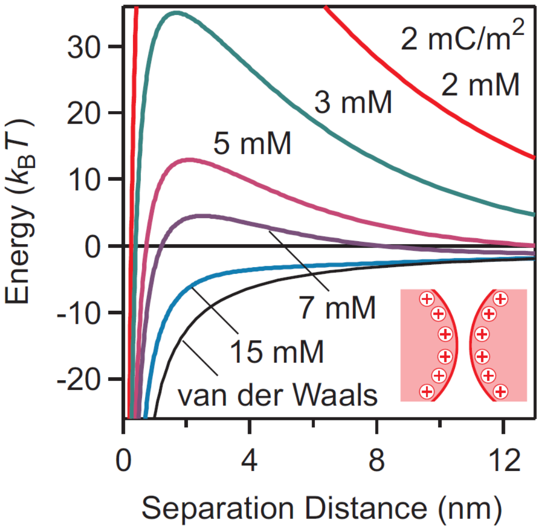

Figure 2.5: Potential energy as a function of Separation distance for different salinities as shown by [23].

Furthermore, Fig. 2.5 and Fig. 2.6 show the dependency of the energy potential on salinities and surface charge densities respectively. As can be noticed, the double layer contributions is dominating at low salt concentrations and at high surface charge densities, determining an attractive potential energy profile; on the contrary, at high salt concentration, the VdW forces prevail since, due to the high electrolyte concentrations, the surface of the particles are surrounded by charges that shield the repulsive effect of the double layer interaction [24].

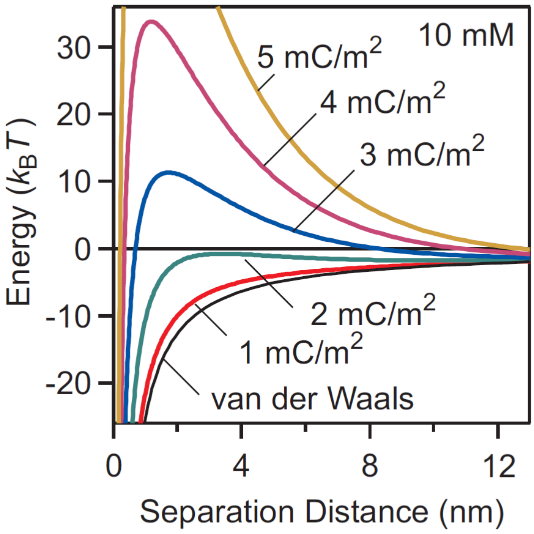

Figure 2.6: Potential energy as a function of Separation distance for different surface charge densities as shown by [23].

The concept of critical concentration of coagulation ccc is also considered by [22]. In particular the the theory affirms that the rate of coagulation N is the given by the ratio between the rate of coagulation due to diffusion N_c and the stability factor W_c:

$$N = \frac{N_c}{W_c} \tag{2.14}$$

$$W_c = 2a \int_{2a}^{\infty} e^{\frac{V}{kT}} \frac{dr}{r^2} \tag{2.15}$$

Where V is the potential energy between the two bodies, which are simplified as ideal particles of radius a, which are divided by a distance R. There is a sharp transition between the significant coagulation behavior (W_c close to 1) and the slow coagulation behaviour (W_c above to 10^5) [25]. This rapid shift allows to determine the CCC, defined as the salt concentration that significantly increase the coagulation behaviour in a colloidal solution. Examples of real application of the CCC will be given in the following sections.

Particle-membrane interaction

The DLVO theory so far introduced, describes the interactions between two surfaces in a water solutions not considering the mass transport phenomena, essential aspect in the study of membrane fouling. Therefore, in the following paragraphs, the focus will be shifted on determining the interactions between particle and membrane surface, considering both the chemical and the physical phenomena of the problem.
Bacchin *et al.* in their work [26] [27], represent the net flux of particles to the membranes N, as composed of a convective term (a), a diffusive term (b) and an interaction induced migration term (c). The fluidodynamics of the solution will be responsible for the drag force on the particle, thus determining the convective term, while the surfaces interactions will be responsible for the remaining two terms:

$$N = \underbrace{J\Phi}_{a} \quad \underbrace{-D\nabla\Phi}_{b} \quad \underbrace{-\frac{D}{kT}\Phi\nabla V}_{c} \tag{2.16}$$

In the formula above, Φ is the colloid concentration, J represents the hydrodynamic velocity of the fluid, D the diffusion coefficient, k the Boltzmann constant and T the absolute temperature. In these works, V represents the energy potential, which is possible to deduce from the DLVO theory of section 2.3.3.
Following the pore scale analysis above, a new definition for the critical flux , already discussed previously, is introduced; indeed it is possible to interpret J^* as the flux at which the three terms, a, b and c are perfectly balanced; below this value no particle deposition is encountered since the drag force is not able to dominate the repulsive forces between particle and membrane.
J^* can therefore be written as:

$$J^* = \frac{D}{\delta}\ln\frac{V_b}{\delta} \tag{2.17}$$

Where δ is the mass boundary layer thickness, while V_b represents the potential energy barrier established by the DLVO theory.
Alternatively it is possible to express the critical flux in terms of critical Pe number:

$$Pe^* = \ln\frac{V_b}{\delta} \tag{2.18}$$

Adding Particle-Particle interaction

It becomes relevant at this point to introduce to the analysis so far described, along with the particle-membrane, also the particle-particle interactions. As highlighted by [26] it is possible to introduce this effects by using the equation 2.16 with a proper diffusion coefficient, called "collective diffusion coefficient".

It is possible to describe this coefficient as a function of Φ, the particle-particle interaction potential V, the particle volume V_p and the osmotic pressure Π, through the generalized Stockes-einstein equations [28] [29]:

$$D(\Phi, V) = \frac{K(\Phi)}{6\pi\mu a} V_p \frac{d\Pi}{d\Phi} \tag{2.19}$$

In particular Π is an equilibrium property and it is typical of the colloidal dispersion and can be defined as [30]:

$$\Pi = \underbrace{nkT}_{a} \underbrace{-\frac{2\pi}{3} n^2 \int_0^\infty r^3 g(r) \frac{dV}{dr} dr}_{b} \tag{2.20}$$

The first term (a) in equation 2.20 refers to the to the osmotic pressure in the dilute scenario, while (b) is the additional term due to the particle-particle interactions. Therefore it is possible to rewrite the equation 2.16 considering the collective diffusion coefficient in the membrane direction z as:

$$N = J\Phi - D(\Phi, V) \frac{d\Phi}{dz} = J\Phi - \frac{K(\Phi)}{6\pi\mu a} V_p \frac{d\Pi}{dz} \tag{2.21}$$

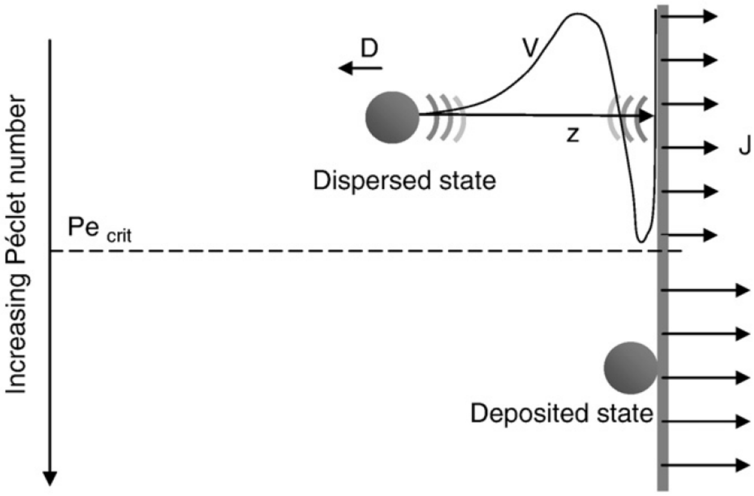

Figure 2.7: Graphical representation of the membrane-colloidal particle interactions as shown in [26].

In analogy with section 2.3.3 a critical flux can be defined as the minimum flux at which the membrane starts presenting a solid phase (fouling). This critical flux is associated to a specific Pe number, which is the limit between disperse and deposited states (Fig. 2.7) and which, for the specific case of dead end filtration, is defined as [31]:

$$Pe_{de_{crit}} = \frac{JV_a}{D} = \frac{V_p}{kT} \int_{\Pi_b}^{\Pi_{crit}} K(\Phi) d\Pi \tag{2.22}$$

Where V_a is the accumulated mass of particles.

Examples of pore scale fouling investigations

In the following sub-chapter, three main experiments, which utilize the theory so far described, will be analyzed. In particular the first one will focus on the interactions with salt and a specific fouling material (bentonite), the second one will study the effects of membrane conditioning on fouling, while the third one will shed some light on the deposition area of single particles on a pore.

1. **Interaction between Bentonite and KCl**
   Bacchin *et al.* [32] offer a valid insight on the filtration and fouling behavior of a bentonite-KCl solution. The relevance of this article is due to the many common elements between the setup and the one utilized in this work, which will be described in the following chapters. The membrane used is made of 24 polysulfone hollow fibers, with a nominal cutoff of 300 kDa, for a total area of 0.024 m^2. The foulant chosen is bentonite, added to water with a concentration of 30 g/L, with a particle size of 700 nm, which is completely rejected by the membrane module. KCl is also introduced in the solution with different concentrations.
   Through their experiments, the authors adopt equation 2.4, considering the effects of osmotic pressure due to concentration polarization negligible , and describing R_{irr} and R_{riv} as a single cake resistance R_c:

   $$J = \frac{\Delta P}{\mu(R_m + R_c)} = \frac{\Delta P}{\mu(R_m + \alpha M_d)} \tag{2.23}$$

   As it is possible to notice from the equation above, R_c could also be considered as the mass of foulant forming the cake M_d, multiplied by the specific cake resistance α.
   The bentonite utilized in [32] is made of platelets which can be modeled as fissure with length L, depth l, thickness e and inter planar distance d_i. Considered the geometry of the foulant two different ways are adopted for describing α:

   $$\alpha = \frac{3(1-\epsilon)}{\rho_s(1-\epsilon)} \left(\frac{2}{e}\right)^2 \tag{2.24}$$

$$\alpha = \frac{5(1-\epsilon)}{\rho_s \epsilon^3}\left(f\frac{3}{a}\right)^2 \tag{2.25}$$

The equation 2.24, where ϵ is the porosity defined as $\epsilon = \frac{d_i}{d_i+e}$, considers the bentonite fissures model for linking the specific cake resistance to the porosity and the particle size. The alternative approach is given by the modified Kozeny-Carman equation 2.25, which considers an equivalent spherical packaging model. In this approach, since the parameter measured through laser light scattering is the volume, the thickness 'e' is related to an equivalent sphere radius 'a' through 2.26; furthermore, a shape correction factor 'f' is required and it is defined by [33] as the ratio between a particle surface and a sphere surface which has the same volume as the particle. For the geometry analyzed by [32], f=9.09.

$$e = 3\sqrt{\frac{4\pi}{3\cdot 10^4}}a = 0.075a \tag{2.26}$$

The authors identify, among others, three main results in their work:

- **Measurement of CCC**
  The salt critical concentration of coagulation (CCC) has been highlighted for the specific application study of the bentonite and salt solution. In particular the particle diameter has been measured for different salinity concentrations as shown in Fig. 2.8. As it can be noticed the particles present a constant dimension until a specific salinity value (CCC) which is around 10^{-2}M. At that concentration the attractive forces describe in the DLVO theory prevail on the double layer repulsive forces, causing the coagulation of the colloidal solution.
- **Specific cake resistance as function of salinity**:
  The specific cake resistance is shown to be dependent on the cake packing characteristics through the parameter ϵ and on the size of the particles that compose the cake. In particular, porosity and particle size are functions of salinity concentrations, allowing to divide the specific cake resistance trend presented in Fig. 2.9, in three main phases. In the first, until 0.001 KCL(M), α remains constant since there is not significant change in either the porosity or the bentonite size. The second part sees an increment in the resistance value due to a decrease of the of the cake porosity. Finally, starting from a concentration of around 0.005 M, α starts decreasing since the experiments show that the average bentonite particle size increases for those concentrations.

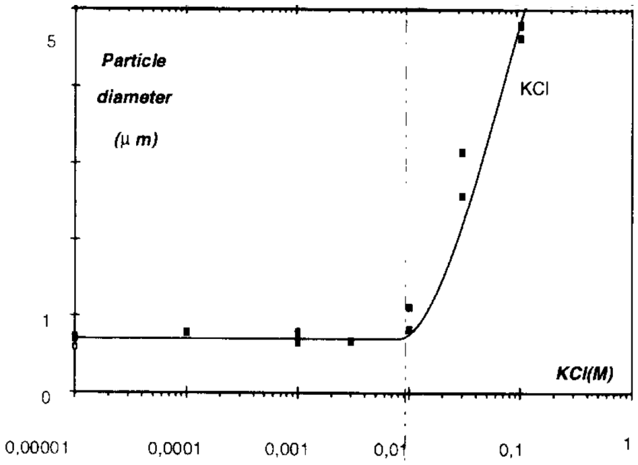

Figure 2.8: Particle diameter as function of salinity concentration as shown in [32], experimental results (dots) are compared to the model prediction (lines)

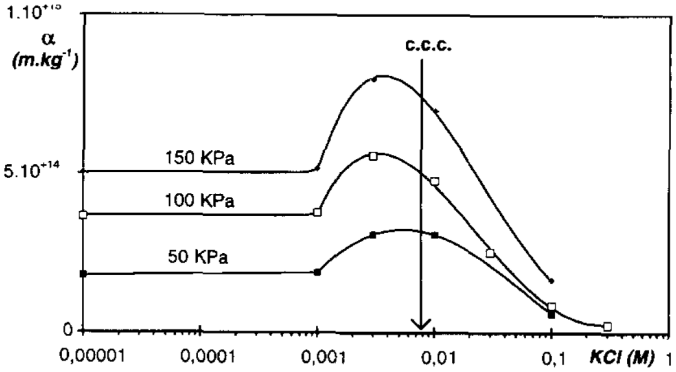

Fig. 5. Specific resistance of the colloid cake versus salt concentration.

Figure 2.9: Specific cake resistance as function of salinity concentration as shown in [32], experimental results (dots) are compared to the model prediction (lines).

- **Cake salt retention** The cake formation also introduces a salt retention capability to the membrane, which has been measured in Fig. 2.10, where the experimental values for different pressures (dots) have been confronted with the model proposed in the work with different inter particle distances (dashed lines), showing a significant correspondence between the two. As it can be noticed, the retention capacity of the cake is strongly influenced by the salinity concentration of the solution; indeed, a higher salt concentration, is followed by a decrease in the strength of the interaction between the ions and the cake layer, which weakens the salt retention capability of the system.

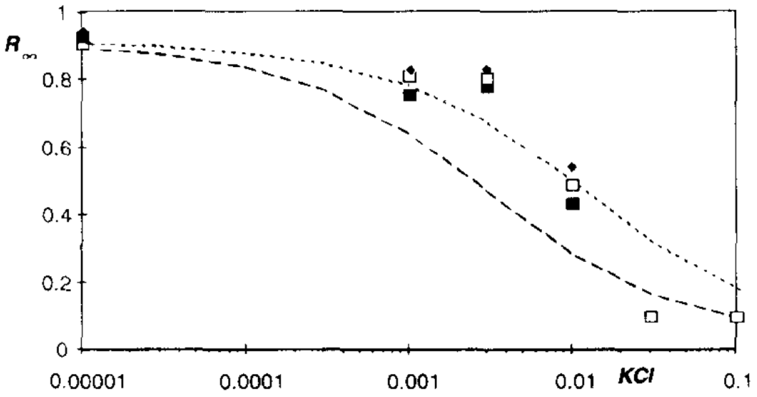

Figure 2.10: Maximum retention coefficient as function of salinity concentration as shown in [32], experimental results (dots) are compared to the model prediction (lines)

2. **Membrane surface conditioning effects on membrane fouling**
   The second relevant study that is now proposed [26] explores the results of modifying the membrane surface properties on colloidal fouling. In particular the deposition area of the fouling particle will be analyzed and justified.
   The fouling material used is polystyrene microspheres (latex) which has been added to water and to a KCl water solution, reaching a volume fraction of $10^{-}3$. The KCl concentration in the solution was set to values ranging from $10^{-}5$ and $10^{-}1$. The measured particle diameter was 4.9 ± 0.21 μm. Furthermore the surface negative charge was measured to be corresponding to a zeta potential of -57 ± 5 mV at ph 7.
   The membrane has been simulated with PDMS micro-separators; this particular structure, made with a soft lithography technique, allows to have full control on the membrane dimensions. In particular 27 parallel micro channels have been chosen, each of them $200\mu m$ long and with a series of 4 restrictions $20\mu m$ wide in their narrowest part (Fig. 2.11 and 2.12).
   The dead end filtration mode has been chosen for the experiments, with a constant filtration flow rate of 2 $\frac{mL}{h}$.
   The conditioning process consisted of rinsing the membrane before every filtration with a $10^{-}1$ KCl solution or with ultrapure water. In the case of the so called KCl conditioning, the estimation of the wettability with the sessile drop, shown an increase of the hydrophilicity of the membrane, while rinsing with pure water shown a more hydrophobic behavior.

   As shown in Fig. 2.11 and 2.12, a small change in the membrane surface properties leads to a significant change in fouling behaviour. In particular, concerning

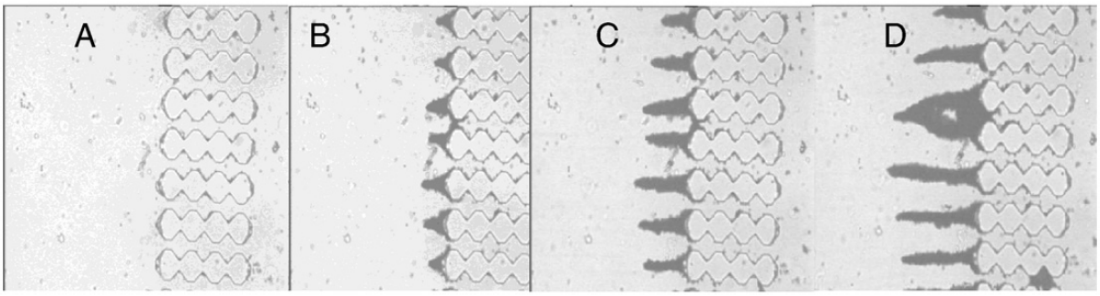

Figure 2.11: Fouling behavior in the case of KCl conditioning as shown by [26];(A) shows $t = t_0$+1 min, (B) $t = t_0$+20 min, (C) $t = t_0$+45 min, (D) $t = t_0$+90 min.

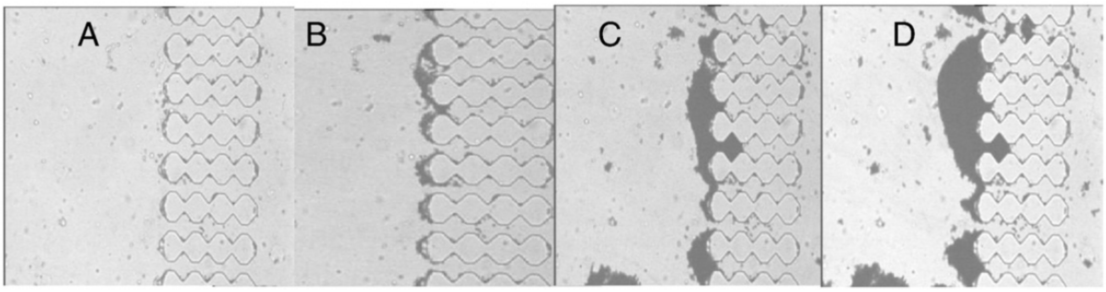

Figure 2.12: Fouling behavior in the case of water conditioning as shown by [26];(A) shows $t = t_0$+1 min, (B) $t = t_0$+20 min, (C) $t = t_0$+45 min, (D) $t = t_0$+90 min-

the KCl conditioning case, the hydrophilicity of the membrane causes the formation of dendrites that can be 40 particle diameters long ($200\mu m$) after 90 min, while the membrane under pure water conditioning experiences arch formation. Considering the effects of different fouling behavior on filtration performance, the dendrites present in Fig. 2.11 don't cause a significant pore obstruction, while the formation of foulant arches in Fig. 2.12 leads to cake deposition, which, keeping the flux constant, causes an increase in operating pressure (TMP).

3. **Particle deposition area**
   The third and last work that is now discussed in this chapter is the work of Lin *et al.*. [34]. In this study, the behavior of fouling particles of size smaller then the membrane pores will be analyzed, with particular focus on the foulant deposition areas.
   This research utilizes as membrane a rich silicon nitride (Si_xN_y) layer on top of a silicon oxide layer (SiO_2), respectively 0.8 μm and 0.7 μm thick. Three different patterns (Fig. 2.13) have been made for the experiments, through a standard mask lithography technique.

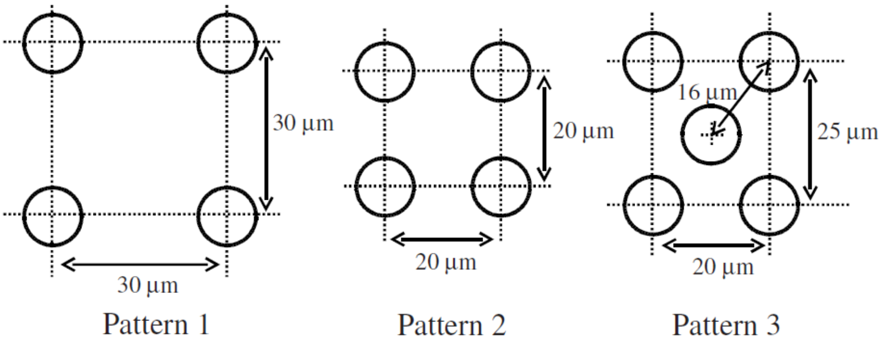

Figure 2.13: Three different membrane patterns chosen for the experiments as shown by [34].

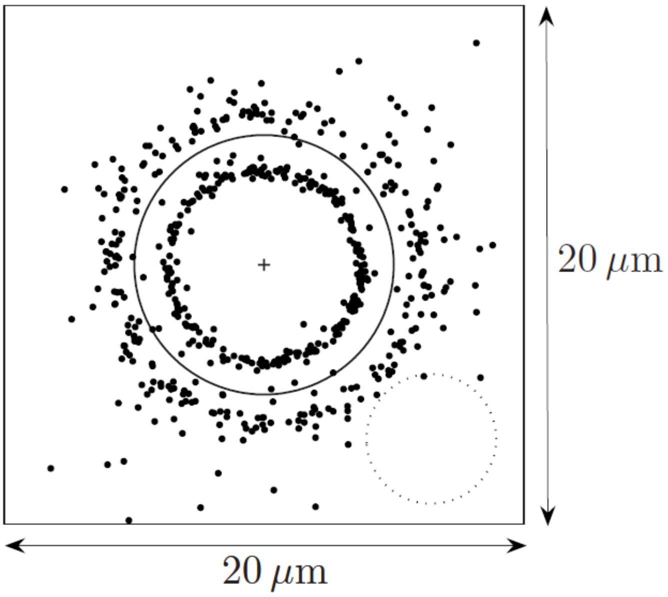

Figure 2.14: Representation of the location of the deposited particles (dots) on the membrane pore as shown by [34].

The solution used for filtration is made of polystyrene microspheres (latex), in KCl-deionized water solution. In particular two different diameters for the foulant particle have been selected: 2.1±0.13 μm and 5.2±0.29 μm. The KCl concentration adopted in water is $10^{-}3$M, while the foulant volume fraction depended on the particle size: 2X10^{-5} and 10^{-5} for the 5.2μm and 2.1 μm diameters respectively.
The filtration flow has been kept constant to values in the range of $5 - 50\frac{\mu L}{min}$ with a precision syringe pump.

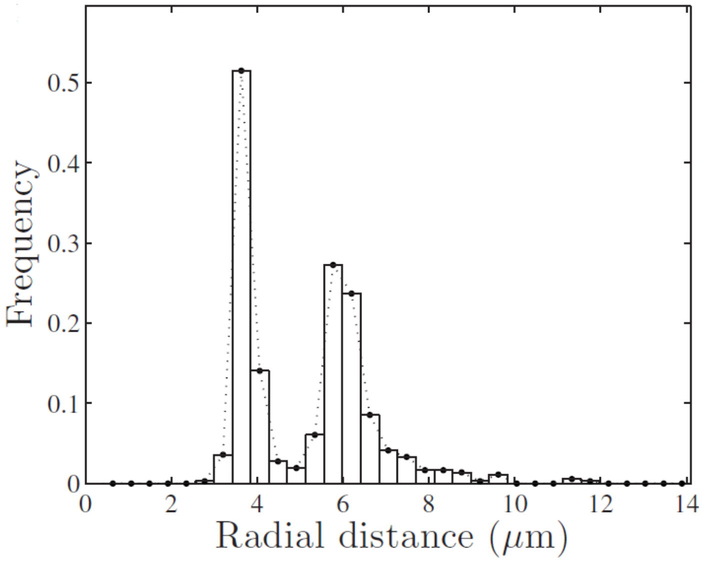

Figure 2.15: Deposited particle distribution as a function of the particle center of mass distance from the pore center as shown by [34].

The main result achieved by [34] can be deducted by Fig. 2.14: independently from the particle size or the membrane pore patterns, there are two preferential deposition areas or, more precisely, two preferential radial distances between the particle centers of mass and the pore center are identified: 3.7 μm and 6 μm. The existence of these locations is described by the authors as the position where the attractive forces (short range vdW) acting between the membrane and the particle are able to overcome the repulsive ones (DL).

Another important investigation has been conducted on the proportion of the particle distribution between the two preferential locations shown in Fig. 2.15. On the contrary of the radial locations, this deposition frequency on one or the other position is strongly influenced by the permeation flow. Indeed, the increase in fluid velocity in the pore proximity, due to an increase in the imposed flow, causes a higher drag force acting on the fouling particle; therefore a higher drag force in proximity of the inner preferential location is expected to increase the capability of the attractive forces to overcome the repulsive forces, causing a higher particle deposition.

2.4 Cleaning methods

After having explored the main flux decline modes, in the following section a brief overview of the flux restoring solutions will be presented. In particular the main mechanisms of physical and chemical cleaning will be analyzed, focusing on the relevant applications and to their effectiveness for different foulants.

2.4.1 Physical Cleaning

In general, membrane physical cleaning is the process that consists in removing the reversible fouling materials through a physical force, which could be related to mechanical, electrical or hydraulic mechanisms [11].
Specifically, as far as water treatment is concerned, the main three physical cleaning methods commonly practiced (separately or combined) are backwashing, membrane relaxation and air scouring [11]. The introduction to these methods found below, will be followed by a review of different case studies on the topic in chapter 3.

Membrane Relaxation

Membrane relaxation consists in interrupting for a specific amount of time the filtration of the membrane setup. This time frame allows the foulants deposited on the membrane to diffuse back the into the solution, due to the concentration gradient at the membrane surface. This solution does not require auxiliary set ups or additional energy. The foulant removal effectiveness of relaxation is usually limited and it is commonly applied in combination with other cleaning methods [35].

Air Scouring

In principle, air scouring (Fig. 2.16) is the cleaning mechanism that introduce an air flux (continuously or intermittently) on the membrane surface in order to avoid foulants to accumulate on the membrane surface or to detach the already existing fouling layer, increasing the membrane productivity [11]. Due to the complex fluidodynamics of the three phases boundary layer created on the membrane, the exact cleaning mechanics of this method is yet to be completely understood.

Backwashing

Backwashing is the process of reversing the permeation flux on a membrane system in order to loosen or detach the fouling layer accumulated on the external part of the filtrating surface [37]. This is a well established technology in industry for its relatively easy implementation and amortization within established parameters; in particular [38]

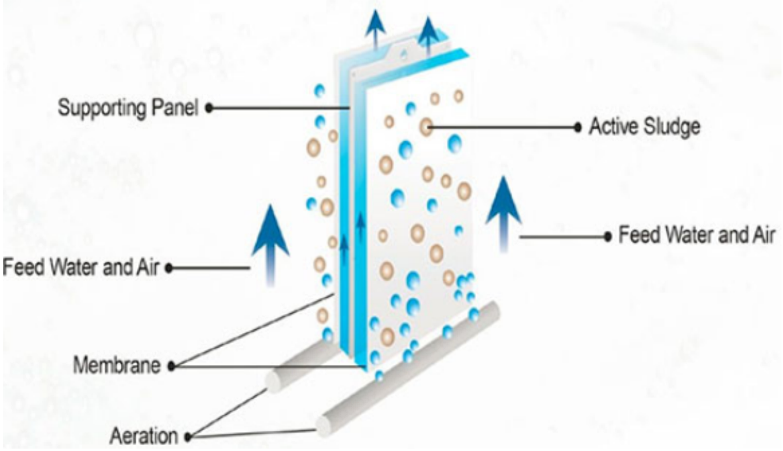

Figure 2.16: Air scouring in a submerged flat membrane as illustrated in [36].

found that most drinking water treatment plant in Germany use as backwash water the permeate produced during the normal filtration functioning, with regular intervals within 10-120 min. A classic example of Backwash is illustrated in Fig. 2.17.

Different combinations of the three methods

In their work De Souza *et al.* [35] offer a valid comparison on the effectiveness of the possible combinations of the different cleaning methods.
The experimental setup used a UF hollow fiber membrane, with a pore diameter of 0.04 μm.
The feed water adopted was simulating real surface water source with: humic acid (3 mg/L TOC), cellulose (3 mg/L TOC), kaoline clay (until achievement of 20 NTU), $CaCO_3$ (150 mg/L), sodium bicarbonate (67 mg/L) and calcium sulphate (129 mg/L). The feed water flow was set to 30 ml/min with with a pressure in the range of 0-0.6 bar. The experiments were set up allowing all the possible combinations of the cleaning methods, within the following operational parameters:

- Air flow: 5 LPM or 15 LPM;
- Relaxation duration 5 min or 15 min;
- Relaxation frequency 4 h;
- Backwash duration: 10 s or 20 s;
- Backwash frequency; 15 min;
- Backwash flux: 19 LMH.

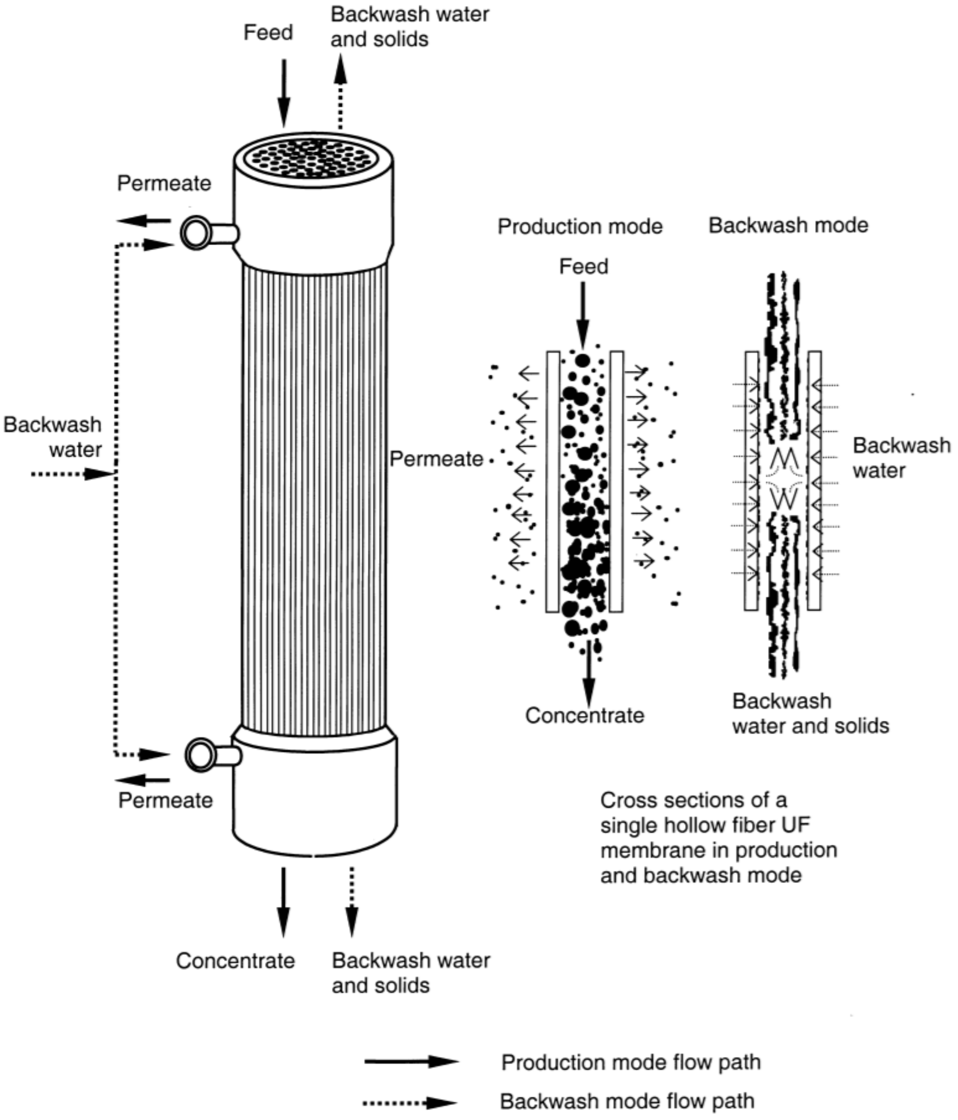

Figure 2.17: Backwash schematics for a cross flow hollow fiber membrane as shown by [39].

As far as fouling removal is concerned, the extended results shown in Tab. 2.1, highlight that the best case scenario is achieved with the combination of high air scouring (15 LPM), short relaxation duration (5 min) and long backwash duration (20 s), showing the lowest final ΔTMP (-8.96 mbar), a high produced permeate (41 L) and the highest specific flux (4.27 LMH/mbar). On the other hand, the worst results have been achieved for low air flow (5 LPM), short relaxation (5 min) and for any of the two values of backwash duration. Generally, air scouring demonstrates a dominant role in fouling removal,

Backwash Duration (s)	**Continuous air flow rate (LPM)**	**Relaxation duration (min)**	**Relaxation frequency (h)**	**Final ΔTMP (±2.6 mbar)**	**Permeate produced (L)**	**Specific Flux (LMH/mbar)**
10	5	5	4	-50.9	41.6	0.75
10	5	15	4	-23.9	40.0	1.60
10	15	5	4	-32.5	41.6	1.18
10	15	15	4	-11.2	40.0	3.42
20	5	5	4	-48.7	41.0	0.79
20	5	15	4	-15.1	39.4	2.54
20	15	5	4	-8.96	41.0	4.27
20	15	15	4	-14.9	39.4	2.57
10	5	5	4	-32.8	41.6	1.17
0	5	5	4	-99.8	42.3	0.38
10	0	5	4	-207	41.6	0.19
10	5	0	4	-82.2	42.5	0.47

Table 2.1: Experiments with different cleaning method combinations, with relative results as shown by [35].

since experiments with low air flow presented higher fouling regardless of the backwash duration. The latter, indeed, is shown to be fully dependent on the other two cleaning modes parameters.

2.4.2 Chemical cleaning

Chemical cleaning is the process that utilizes different types of additives in order to restore the original membrane permeation, after irreversible fouling occurred [41]. In general, as it is illustrated in Fig. 2.18, chemical cleaning can be divided in 6 chronological steps [42]. At first, the bulk reaction between the introduced additive and the fouling layer occurs, followed by the transport of the cleaning agent on the membrane surface. In the third and forth step the additive is firstly transported within the fouling layer and then it interacts with the foulant, determining its detachment from the surface, followed by its transport in the bulk solution.

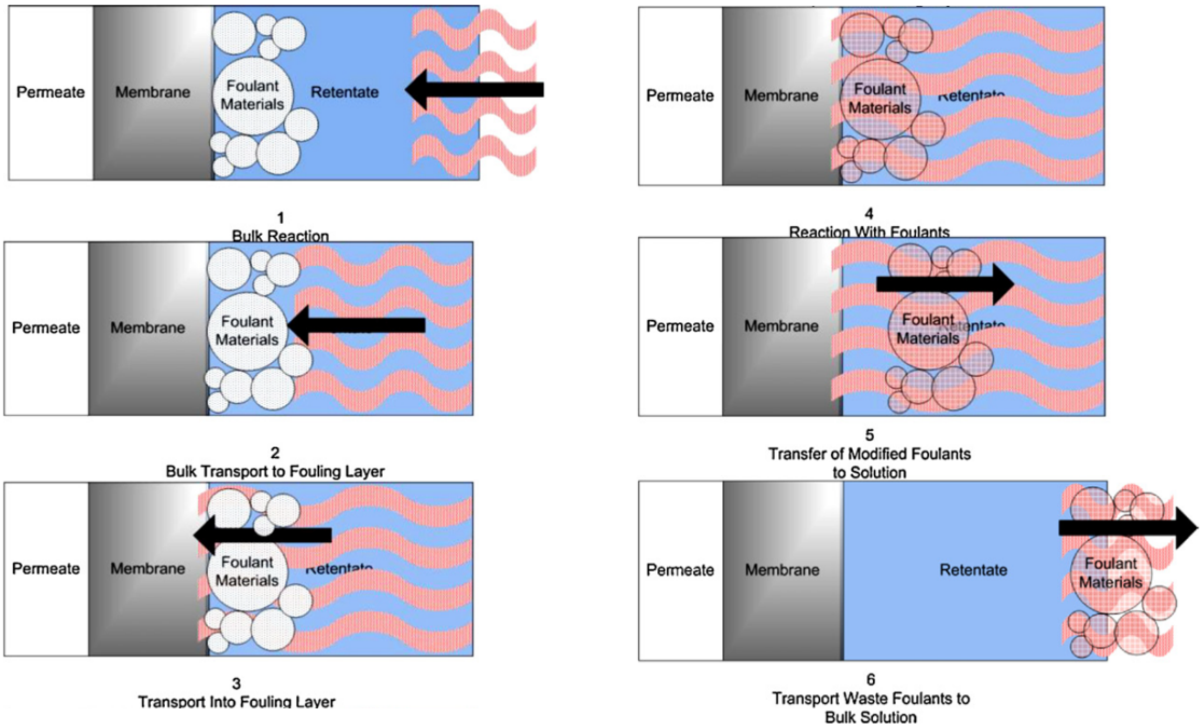

Figure 2.18: The 6 steps of chemical cleaning as illustrated by [40].

Chemical cleaning designs

The two main ways to perform chemical cleanings are the so called CEB (Chemically enhanced Backwash) and CIP (Clean in place) [41]. The first consists in adding particular chemicals to the routine backwash procedures, while the latter requires the removal of the membrane in order to allow its soaking in a chemical bath. Usually, CEB requires a lower additive concentration compared to the one used in many CIP designs, with shorter soaking time and frequent application. In general CEB is used for keeping the membrane performance as constant as possible during the filtration process, while CIP is used to restore the original membrane permeability.

Common Additives

Many additives are commonly used for CEB and CIP and are commercially available. One of the most used chemicals for membrane cleaning is caustic soda (NaOH), since it helps the dissolution of organic particles and it increases the spacing between NOM, determining an easier mass transport within the fouling layer [43]. Also oxidants like NaOCL are used as cleaning additives; indeed, the NOM oxidation increases its hydrolysis in a high ph ambient, determining an easier to remove fouling layer [44].

Furthermore, acids, in particular mineral acids, are used in order to remove ions from hardness salts, also due to their low cost and common availability [45].

2.5 Energy considerations

Depending on the membrane application field or location, electrical energy could often be not steadily available (i.e. renewable energies), expensive or not easily reachable. In these cases energy consumption plays a determinant role in the design choices of a certain technology. It is then relevant in this section to highlight some considerations on the different energy consumption of the main physical cleaning solutions, with some insight on the identification of the energetically optimal backwash duration an frequency.

2.5.1 Energy consumption comparison between membrane physical cleaning methods

A relevant energy comparison between different membrane backwash implementation is given by [46]. In their work, the Canal du Midi (Toulouse, France) water is ultra filtered at a contant flux of 80 $\frac{L}{hm^2}$, through a membrane with a nominal pore size equal to 10 nm and a total filtration area of 6.5 m^2.
Three different cleaning methods have been tested:

- **Conventional Backwash (BW)**
  Permeate water has been used for the backwash phase. The BW flux utilized is constant and equal to 450 $\frac{L}{hm^2}$. The cleaning duration has been fixed to different values for each cleaning protocol in order to reach the same net permeate flux (55 $\frac{L}{hm^2}$) in each method.
- **Air Assisted Backwash (AABW)**
  The backwash phase is enhanced by the injection of air in the membrane module with a constant gas velocity of 0.54 $\frac{m}{s}$. The duration of this cleaning phase is determined analogously to the traditional BW.
- **Air assisted Backwash with preliminary rinsing (AABW + Rinsing)**
  A rinsing step is added prior to the BW phase. The rinsing of the membrane is carried out with a total of 16.5 L of raw water, flushed on the membrane during 105 s.

The energy consumption is calculated also taking into account the different permeate water losses for each cleaning protocol, which are for example not present in the rinsing step, due to its use of raw water. Also the missed permeate water production due to the

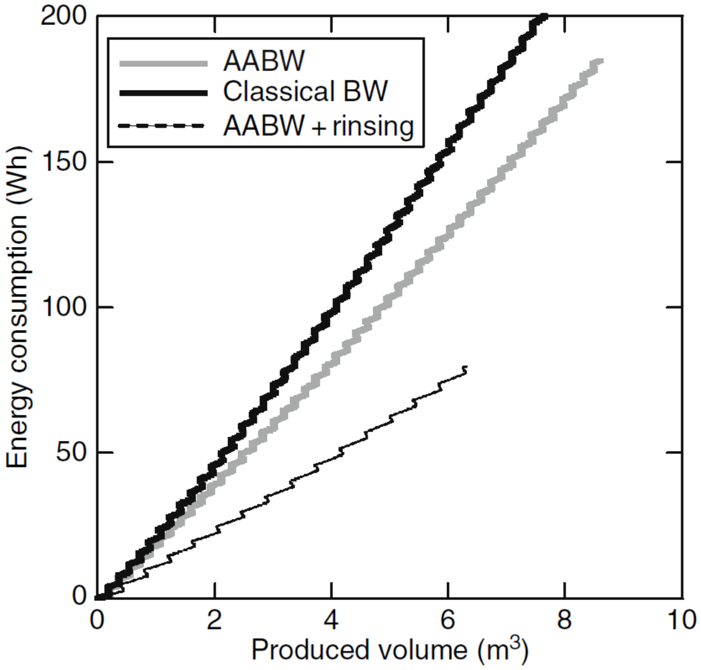

Figure 2.19: Cumulative energy consumption as function of produced volume for the three different cleaning methods as illustrated by [46].

filtration mode pause is considered for the analysis of the results.
The energy consumption comparison between the three methods is shown in Fig. 2.19. As one can see the three trends are diverging due to the cumulative effects of fouling. AABW + rinsing is the most energy efficient method, indeed, 6 m^2 of net permeate water cost, in terms of energy, 22% and 69% less for AABW and AABW + rinsing respectively, compared to classic BW. Then, it is possible to deduce that the increase in energy consumption due to the introduction of the air injection and the raw water pumping in the cleaning phase is less relevant than the lower backwash frequencies and than the higher filtered water consumption.

2.5.2 Backwash energy optimization

One of the most relevant subject in the membrane cleaning energy analysis is the parameters energetic optimization. In particular, in this section, the influence of BW duration and frequency on system consumption will be introduced. In their work, Massé *et al.* [47] test an air assisted backwash setup with different backwash frequencies (5 min, 15 min, 60 min) and durations (10 s, 20 s, 30 s, 50 s, 60 s, 80 s). A solution of pure water and non-refined see salt ($35\frac{g}{L}$) has been filtered by a polysulfone UF membrane (A=0.38m^2) at a constant feed flow rate of 0.8 $\frac{m^3}{h}$.

As it is possible to understand from Fig. 2.20, keeping the backwash frequency constant at 15 min, the optimal backwash duration is equal to 30 s, in terms of both net permeation flux (27 $\frac{L}{hm^2}$) and total specific energy consumption (146 Whm^2). In particular it is very significant to notice the high increase in pumping SEC, going from 22 Whm^2 to 130 Whm^2, when the BW duration increases from 10 s to 80 s.

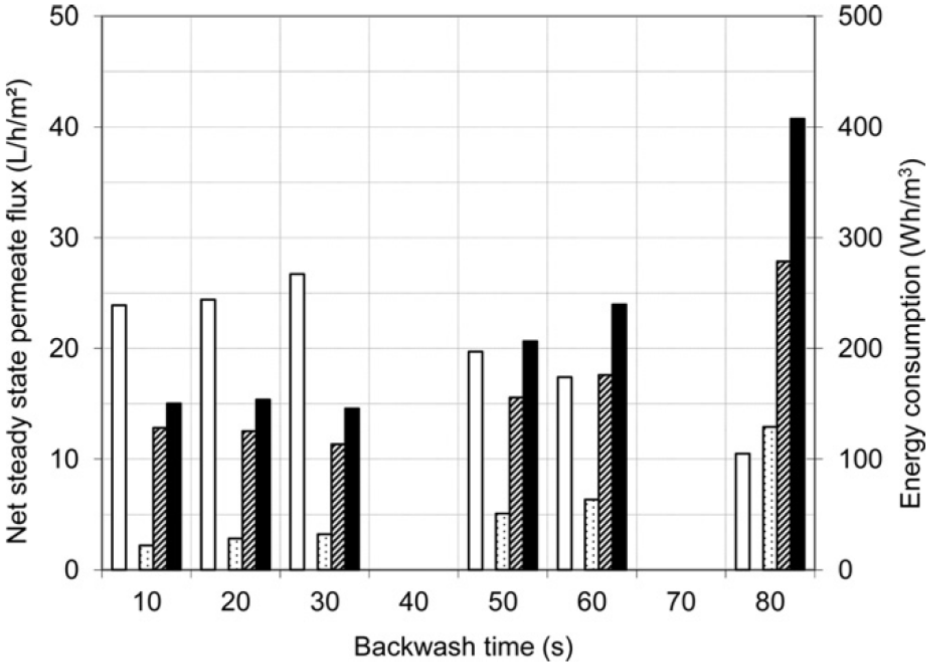

Figure 2.20: Net permeate flux (white bar), bubbling (hatched bar), pumping (dotted bar) and total (Black Bar) specific energy consumption, for different backwash durations as illustrated by [47].

On the other hand, Fig. 2.21 shows the influence of backwash frequency on system performance, at a constant backwash duration (30 s). As far as the net permeate flux is concerned, its maximum value is achieved with a backwash frequency equal to 15 min (27 $\frac{L}{hm^2}$), while the same value of total specific energy consumption is reached by backwashing every 15 min or 60 min. In general then, it is possible to conclude that 15 min is the optimal backwash frequency since, with a similar total SEC compared to the 60 min mode, it is able to achieve a higher net permeate flux.

2.5.3 Relevance of Energy optimization

Another important aspect in the energy optimization concept is to be found in its strong influence on the cost feasibility or design studies of a specific membrane applica-

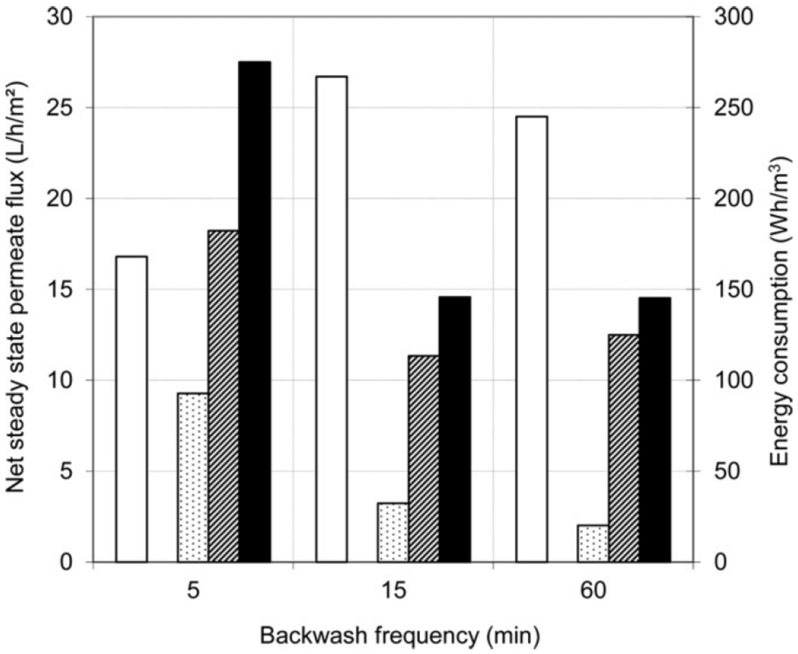

Figure 2.21: Net permeate flux (white bar), bubbling (hatched bar), pumping (dotted bar) and total (black bar) specific energy consumption, for different backwash frequencies as illustrated by [47].

tion. Indeed, energy cost is one of the main contributor to operational cost in many pressure driven membrane applications. Parameshwaran *et al.* [48] in their work highlight this specific role in the system design choices; in particular, the authors, first correlate the membrane imposed flux to the backwash frequency required to keep the filtration TMP below a certain constant value (TMP_{max}) and then they calculate the total system cost (Investment + Operational cost) through the simplified economical data found in Tab. 2.2. The results in Fig. 2.22 show that, since the required backwash frequency is found to be inversely proportional to the imposed filtration flux, the energy cost trend is growing with the flux, on the contrary of capital cost which follows the scaling law. As a consequence of these two opposite trends, the resulting total cost shows a minimum, which is located at fluxes equal to 65 and 80 $\frac{L}{m^2h}$ for values of TMP_{max} corresponding to 2 and 5 bar respectively. In general, it is possible to conclude that presence of the total cost optimal value is strongly influence by the energy consumption optimization of the system, which therefore affects the whole design of the application.

Plant Capacity	1000	$\frac{m^2}{d}$
Cost of electricity	0.15	$\frac{Aus\$}{kWh}$
Capital cost	200	$\frac{Aus\$}{m^3 installed}$
Capital cost distribution (linear)	0.15	$\frac{1}{year}$
Plant operation period	350	$\frac{Days}{year}$
BW Energy Requirement	0.002	$\frac{kWh}{Backwash{*}m^2}$

Table 2.2: Cost analysis parameters, modified from [48].

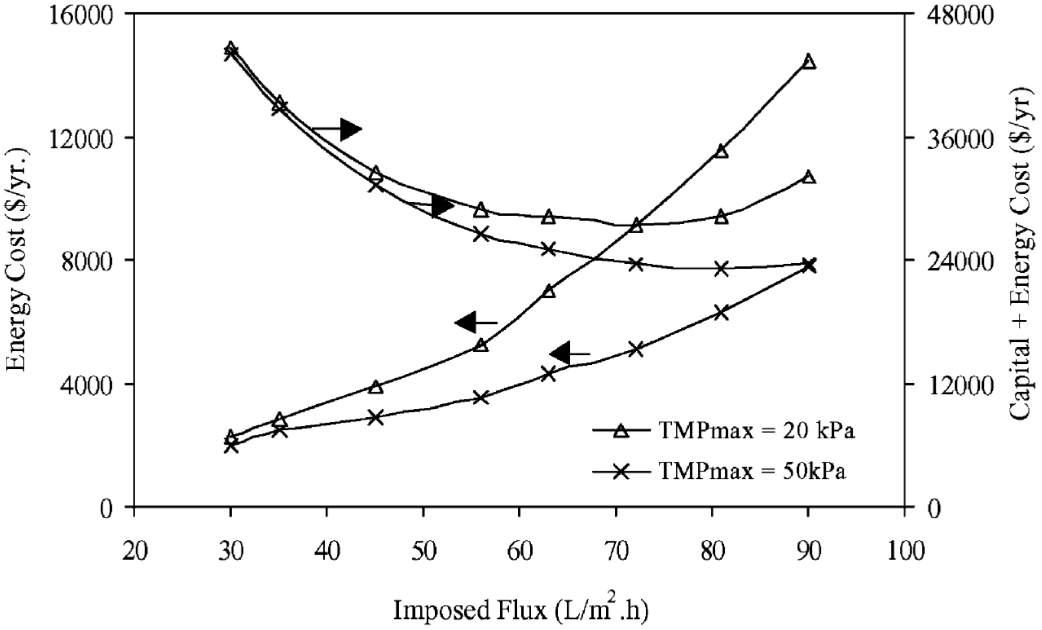

Figure 2.22: Energy cost and Capital cost as a function of imposed permeation flux as illustrated by [48].

2.6 Backwash simulation in literature

Now that the main aspects of membrane fouling and cleaning mechanisms have been introduced, the focus of this section will be to summarize what water additives have been utilized for simulating fouling in relevant research and to collect some of the experimental backwash durations and frequencies commonly used in literature. These final information will be utilized for designing the experimental setup that will be illustrated in detail in chapter3. In general is it possible to affirm that, due to the complexity of the different phenomena involved in membrane fouling, it is difficult to predict how different foulants will interact between each other; organic and inorganic particles show a synergistic effect concerning the irreversible blocking of the membrane. As shown by [15], the flux decrease rate of the experiment with water containing both Kaolinite and Humic acid (HA) is higher than the sum of the individual decrease rates. Therefore, the backwash experiments are often led through real case water filtration or, when fouling is simulated, with single additives that are usually categorized basing on the type of fouling required, which is often organic or inorganic.

UF Organic Fouling

Since Natural Organic molecules (NOM) are commonly found in surface and ground water [49] [50], many experiments are led using NOM as organic fouling substance. Examples are given [51], which utilizes washed yeast and by [52], which employs sodium alginated. A problem derived by the adoption of these additives is the presence of significant irreversible fouling. These behavior is shown also by the above cited experiments; in particular [52] displays a drop of about 20 percent of the initial flux after 7 backwash cycles (7 hours), while the membrane in [51] requires chemical cleaning after 40 hours with a foulant concentration of 500 mg/L. Then, the reproducibility of the experiments is connected to the chemical cleaning mechanism efficiency and to the state of wear of the membrane.

UF Inorganic Fouling

Inorganic fouling is representative of clay particles, which are common in both grey and natural waters [53] [54]. The most used types of inorganic fouling particles are Kaolinite (30, 100 mg/L) [55] [15] [54] and Bentonite (30, 50, 170 mg/L) [32] [56] [57]. Experiments on both small and large scales show that the inorganic fouling is mostly reversible, since the relative large size of the particles (around 500 nm) compared to UF membrane pores (20 nm), avoids pore blocking and pore adsorption. Therefore, in these cases, fouling is dominated by cake formation [56]. Experiments show no relevant membrane degradation in terms of permeate flux and TMP. In particular [55] displays a total 5 percent flux reduction in the first 2 backwash cycles and no further loss in performance for the following hours (8 h Tested). On the other hand [56] and [57] show no irreversible fouling formation for 7 h and 24 h respectively, with backwash cycles of 20-30 s every 30-60 min.

Backwash durations and frequencies

The most relevant parameter values to our research are grouped in Tab. 2.3. It is possible to notice that, on the opposite of duration, which is often set to values close to 30 s, BW frequency has a broad range of values due to the intrinsic high number of potential membrane applications and therefore due to the different possible types of foulants and performance parameter values.

Backwash duration [s]	10	[47], [35]
	20	[56], [47], [35]
	30	[57], [47]
	40	[47]
	50	[47]
	60	[47]
	80	[47]
	120	[55]
Backwash Frequencies [min]	5	[47]
	15	[47], [35]
	30	[54], [56]
	60	[57], [47]
	120	[55]
	150	[54]

Table 2.3: Significant backwash frequencies and durations adopted in literature.

Chapter 3

Methodology

3.1 Materials

The experimental setup (Fig. 3.1) is a UF-RO desalination system. The idea behind such configuration is to extend the life of the RO membrane by preventing its fouling and to guarantee a constant water quality through the use of a preliminary filtration stage, in this specific case represented by the UF element. Indeed the UF detains the suspended particles, pathogens and proteins so that the RO membrane is feeded with clean salty water.

A filtration pump provides the driving pressure for the system; it is connected to a charge controller which is sourced by a solar array simulator (Fig. 3.2). The pump, due to a proper needle valve placed on the concentrate side of the RO membrane, keeps the system pressure to a constant value of 10 bar, since this is found to minimize the specific energy consumption (SEC) of the configuration with high flux and retention [58]. The system is constantly monitored with a Labview software, which, through a data acquisition card, communicates with the multiple sensors located the configuration: pressure, flow, temperature and conductivity (which allow to measure the salt concentration).

Two different backwash systems have been added to the original configuration: the first one is a passive configuration which utilizes a bladdder tank as BW water storage at 4 bar, which is directly provided by the filtration pump and employed when requested; instead, the second setup implements a DC BW pump which can be connected either to a DC power supply (PSU) for preliminary testing or to an array of supercapacitors (Fig. 3.2). The switching between the two configurations is done detaching manually the respective legs in the position indicated by the number 16 in Fig. 3.1, without the use of a three way valve, avoiding the associated pressure drop.

In order to set the filtration and backwash durations in the experiments, the labview program sends the commands to a relay card which is able to control the solenoidal valves and the two pumps of the system.

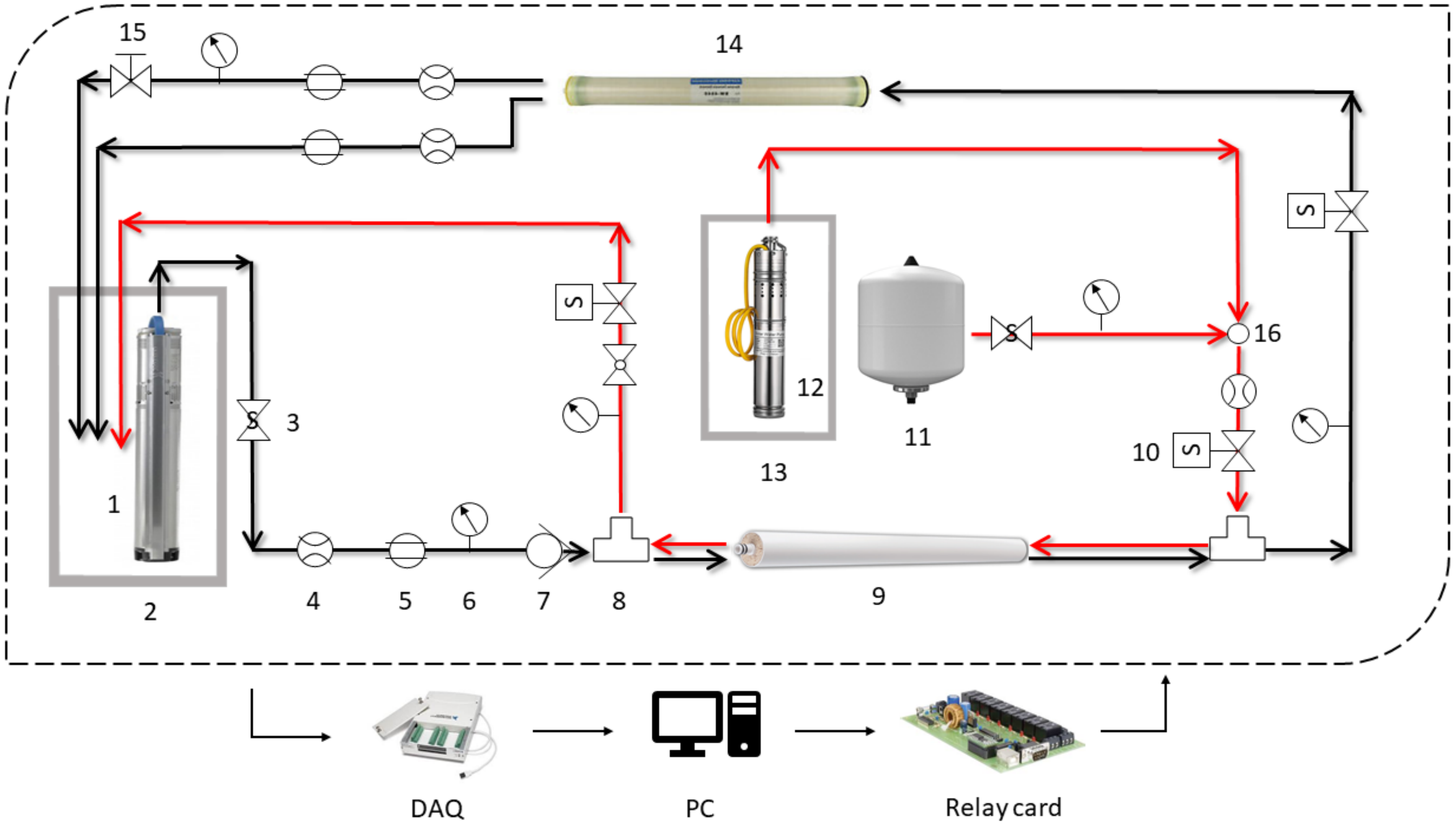

Figure 3.1: System schematics; the black and the red lines indicate the filtration and the backwash loops respectively. (1) Filtration pump, (2) filtration tank, (3) safety valve,(4) flow sensor, (5) conductivity sensor, (6) pressure sensor, (7) check valve, (8) tee fitting, (9) UF membrane, (10) solenoid valve, (11) bladder tank, (12) BW pump, (13) BW tank, (14) RO membrane, (15) needle valve, (16) manual connection point

The water used in the filtration experiments is a brackish water solution, obtained by mixing deionized water with 5 g/L NaCl, in a 250L stainless steel tank and its temperature increase is mitigated by a dedicated chiller. Bentonite is added in order to simulate fouling for the BW set up, with a concentration of 500 mg/L with an average particle size of around 500 nm.

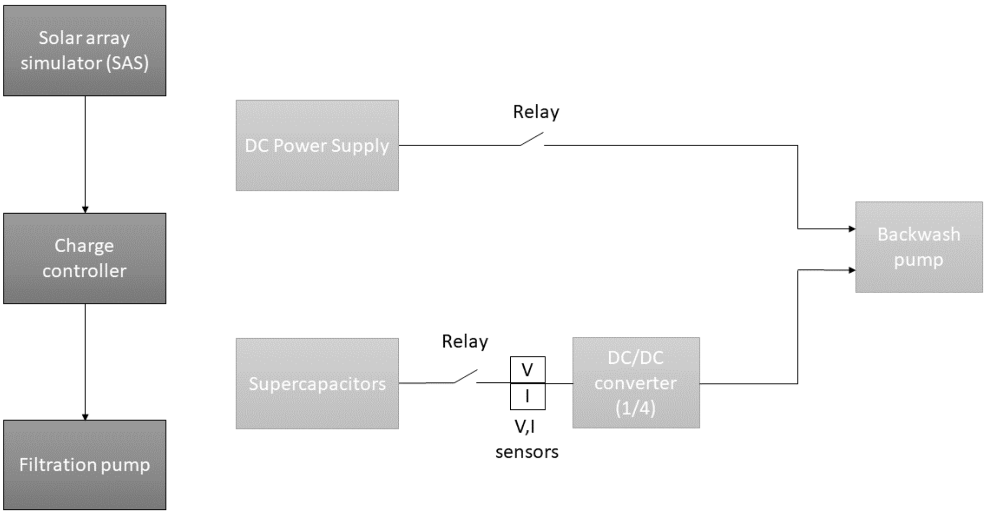

Figure 3.2: Electrical connection schematics for both the filtration and backwash legs.

3.1.1 Backwash system components

- **UF membrane**
  The membrane selected for the ultrafiltration step is the Inge Dizzer P4040-6.0. It is a hollow fiber membrane, made only of Polyethersulphone (PES), with a patented spinning procedure which allows the building of a so called "Integral" membrane, avoiding the creation of different layers and their possible wear due to peeling [59].
  Each fiber combines seven capillaries with the same diameter of 0.9 mm, and it is structured as shown in Fig. 3.3: the inner surface has an average pore diameter of around 20 nm, while the support outer channel support structure has a much larger average diameter pore size, with a 1.000 times higher layer permeability; finally the outer pores measure on average 1 μm.

  The overall membrane module has the following characteristics:

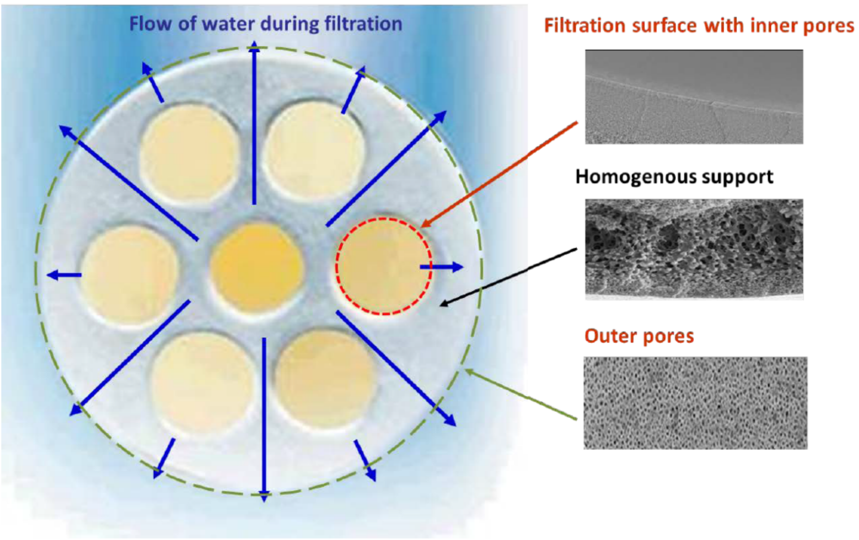

Figure 3.3: Single fiber structure as shown in [59].

- Membrane area: 6 m^2;
- Length: 960 ±1.5 mm;
- Outer diameter: 100 mm;
- Inner diameter: 28.4 mm;
- Weight: 4.5 kg

The module is operated with a dead end filtration mode and it is finally contained in an end port pressure vessel, with a diameter of 4” and a length of 1.197 m. It is made of glass reinforced epoxy resins and can reach a maximum pressure of 41.4 bar.

- **Solar array simulator (SAS)**
  In order to simulate real operating conditions, a solar array simulator (SAS) has been chosen as power supply for the filtration system. The model selected is the Chroma 62050H-600S, which is a programmable DC power supply that allows to simulate real solar days irradiation trends (imported through USB as excel files) and to translate them in voltage and current inputs for the setup.
  The characteristics of the SAS are:
  - Maximum Power: 5 kW
  - Voltage range: 0 - 600 V
  - Current range: 0 - 8.5 A

- **BW tank**
  The tank utilized for storing the backwash water is made of stainless steel against corrosion, has a diameter of 50 cm and a hight of 80 cm. It is filled with 120 L of DI water with 5 g/L NaCl.

- **Fouling Agent**
  Inorganic fouling with a clay material has been selected for the reasons previously introduced in section 2.6. The specific fouling agent is TIXOTON® which is a commercial product manifactured by Clariant [60], introduced in the 250L filtration water with a concentration of 500 mg/L. Such concentration has been chosen since it allows a measurable increase in filtration TMP in relatively short times and it is comparable to value used in previous literature (see 2.6).

- **BW pump**
  The pump chosen for the BW phase is a DC helical rotor pump (model number: s242T-40), which utilizes a permanent magnet motor with a built in maximum power point tracking (MPPT). It is made of stainless steel and has the following specifics:
  - Maximum Head : 40 m;
  - Maximum Flow : 2 m3/hr;
  - Nominal power : 284 W;
  - Voltage Range : 18-45 V.

- **Mixing pump** In order to keep the bentonite from depositing on the bottom of the tank an AC mixing pump has been adopted (Pentair Jung pumpen U3KS/2) with a maximum flow of 6.5 m^3/h and a nominal power 320 W.

- **Power supply**
  The power supply chosen for the preliminary experiment of the BW pump is the model EA-PS 5080-20 A. This is an adjustable PS with the following characteristics:
  - Volage range: 0 - 80 VDC;
  - Current range: 0-20 A;
  - Maximum power: 640 W.

  The output of power supply has been set to a constant value equal to 40 V. The high current required by the BW corresponding to this voltage is the reason that has lead to the selection of a unit able to deliver such a high maximum current.

- **Bladder tank**
  As bladder tank the Sanibel Comfort 6140017 has been selected [61]. It has a nominal volume 8 L and a max operating pressure on the liquid side of 10 bar. The air pressure has been manually set to 1 bar, allowing the pressure on the water side to comfortably reach 4 bar (maximum pressure achievable without applying a UF TMP higher than the security limit set to 3 bar during the BW phase).

- **Supercapacitors**
  A group of 12 supercapacitors with the following characteristics were used as energy source for the BW pump for the second part and third part of the experimental protocol of section 3.3:

  - Maximum operating voltage: 180 V;
  - Internal resistance:228 $m\omega$;
  - Capacitance: 4.83 F;
  - Leakage current: 1 mA;
  - Power density: 3000 W/kg;
  - Maximum energy: 3.63 Wh/kg;
  - Operating temperature range: -40 to +65$°C$.

- **DAQ Card**
  Each sensor comunicates with the Labview software trough a data acquisition cards (DAQ). The model NI-USB 6229 by National instruments has been adopted. This particular DAQ features 32 Analog Input (AI), 48 Digital Input/Output (DIO), 4 Analog Output (AO) and 2 counters channels. It communicates and it is powered through PC USB connection, but requires an external PSU for powering of the sensors. The latters can be implemented in the DAQ through direct measuring of the sensors output voltage or by means of an additional external resistor which translates the output voltage into a current that is then acquired by the card.

- **Sensors**
  A total of 6 sensors, with the relative calibrations, have been added to the existing filtration setup:

  1. **Flow sensor**
     A specific sensor for the BW flow has been installed; specifically a magnetic-inductive flow meter sensor manifactured by IFM (model SM6000) has been selected.
     It is made of stainless steel (1.4404 / 316L) and it shows the following characteristics:

- Measured flow range: 0.1 - 25 L/min;
- Input voltage: 7-33 VDC;
- Output signal range: 4-20 mA or 0-10 VDC;

In our specific case, the sensor voltage output has been converted to a current through the use of a resistor with a known resistance in the DAQ. In order to calibrate the sensor, first, as security check, the amount of water exiting the sensor has been checked to be equal to the value shown by the built-in sensor display, which is factory calibrated; then, ten different flow values (read from the display) have been associated to the corresponding measured output current from the sensor. The equation that describes the relationship between the two quantities is shown in Fig. 3.4 and will be useful for the Labview software calibration in section 3.2.

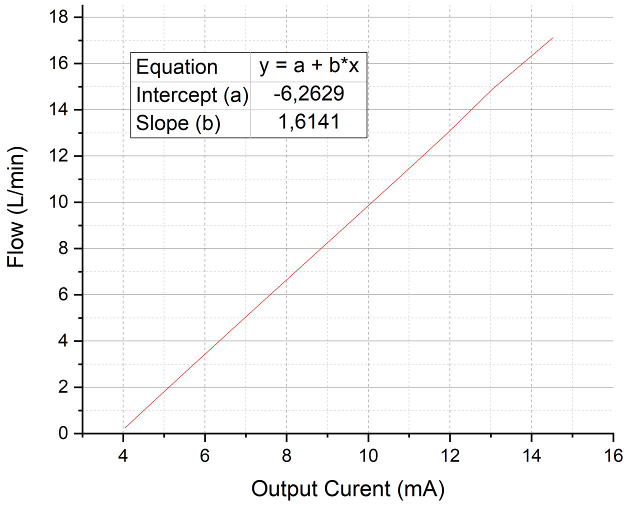

Figure 3.4: Measured flow vs sensor output current for the sensor IFM SM6000.

2. **Pressure sensors**

   Three pressure sensors manifactured by Burkert (model number: 8316) have been included in the BW setup with the following specifics:

   - Pressure range: 0-16 bar;
   - Input voltage: 7-33 VDC;
   - Output signal range: 4-20 mA or 0-10 VDC;

   The wetted part of the sensor are made of stainless steel 316L, which makes them suitable for the required application.

The sensor output voltage has been converted by the data acquisition card into a current with the same procedure described for the flow sensor; the relationship between measured pressure and sensor output current has been plotted in Fig.3.5 and its equation will be utilized for the software calibration in section 3.2.

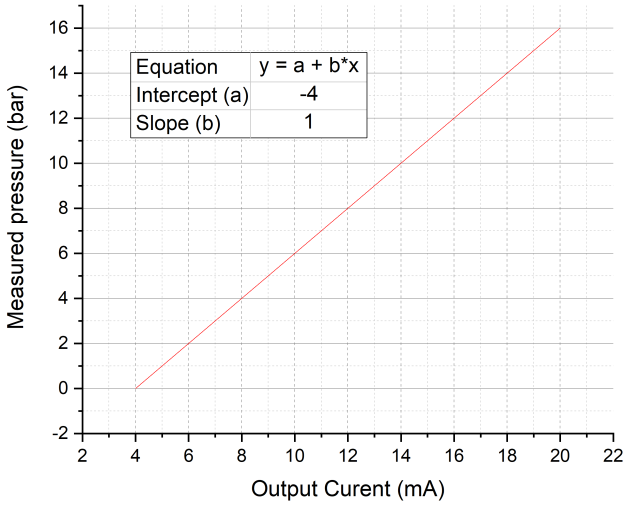

Figure 3.5: Measured pressure vs sensor output current for the sensor Burkert 8316.

3. **Voltage and current sensors**
   In order to monitor the BW pump power consumption a voltage and a current sensors have bee added. They are manifactured by Omega and their model is DRF-VDC and DRF-IDC. They show the follow characteristics:

   - Measured current range: 0 - 5 A;
   - Measured voltage range: 0 - 300 V DC;
   - Input voltage: 7-33 VDC;
   - Output signal range: 4-20 mA or 0-10 VDC;

   On the opposite of the others, the current and voltage sensors have been implemented to the DAQ by measuring directly the output voltage, with no external resistor needed. The calibration has been performed also in this case, with the results shown in Fig. 3.6 and 3.7.

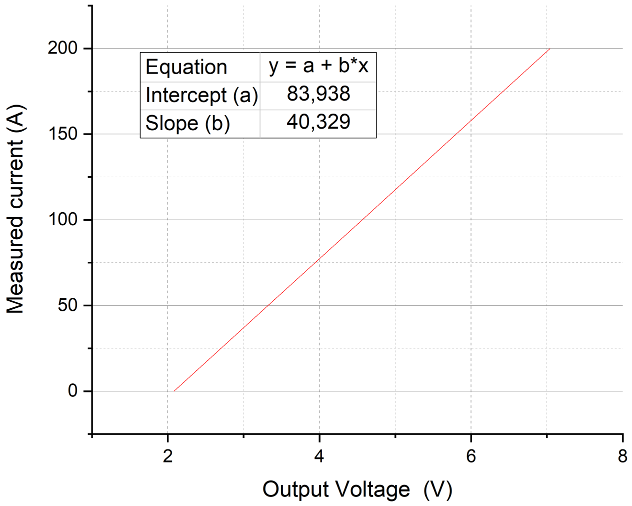

Figure 3.6: Measured voltage vs sensor output voltage for the sensor Omega DRF-VDC.

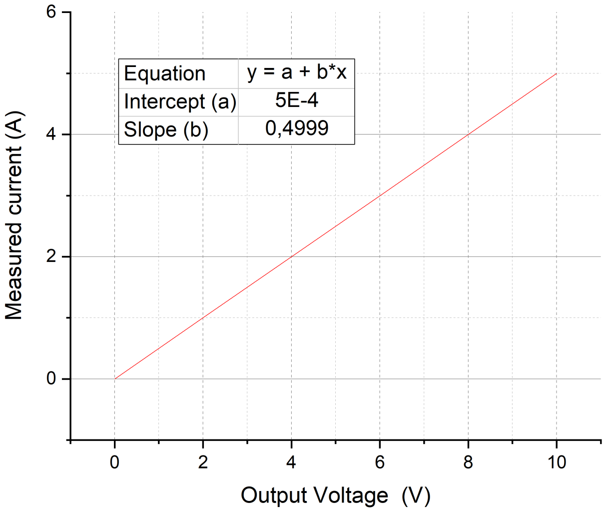

Figure 3.7: Measured current vs sensor output voltage for the sensor Omega DRF-IDC.

- **Valves**
  A total of three solenoidal valves are used for controlling the switching between filtration and backwash modes in the setup. The units chosen are the Burkert 5282, which are electromechanically controlled through a relay card, which de-

livers a current of 4-20 mA at 24 VDC through the solenoid. There are two types of valves chosen for the system: normally open (NO) and normally closed (NC); when the units are energized, they change from one state (open or closed) to the other and viceversa. The working principle used by the valve rely on a magnetic field that is formed when the solenoid is electrified, that causes a plunger inside the coil to move so it can open or close the valve. They are built with stainless steel 1.4581 and can bare a maximum pressure of 15 bar.
In order to ensure that the pressure inside the backwash leg will never exceed 10 bar (as indicated by the bladder tank specifications), a safety valve is implemented in the setup. Such unit (Goetze-armaturen 460) will allow the water to evacuate the system in case of excessive pressure through a dedicated pipe connected directly to the valve.

- **Relay Card**
  The labview software communicayes the commands to the system through the use of a dedicated relay card. The model used is the Conrad 197730 (Fig. 3.8) and has the following characteristics [62]:

  - Number of relays: 8;
  - Serial interface: RS232, 19200 baud, 8 data bits, 1 stop bit, no parity bit, no handshake;
  - Max. current consumption: 400mA at 12V/DC, 250mA at 24V/DC (8 relays activated);
  - Max. relay switching capacity: 230V/DC, 16A or 24V/DC, 16A.

  The relays allow for both a normally closed or a normally open configuration (Fig. 3.8, letter A) and in this application they are used for switching on or off the filtration pump (relay 1, NC), the three solenoid valves (relay 2,3 and 4, NO) and the backwash pump (relay 5, NO).
  The relay communicates with the PC with a USB cable through a dedicated USB converter (Fig. 3.8, letter J). The card requires to be powered by an external PS with a voltage in the range of 12-24 VDC (Fig. 3.8, letter K). Finally a set of jumper connection (Fig. 3.8, letter H and G) allows choosing the card working mode that in this case is set to single card operation.

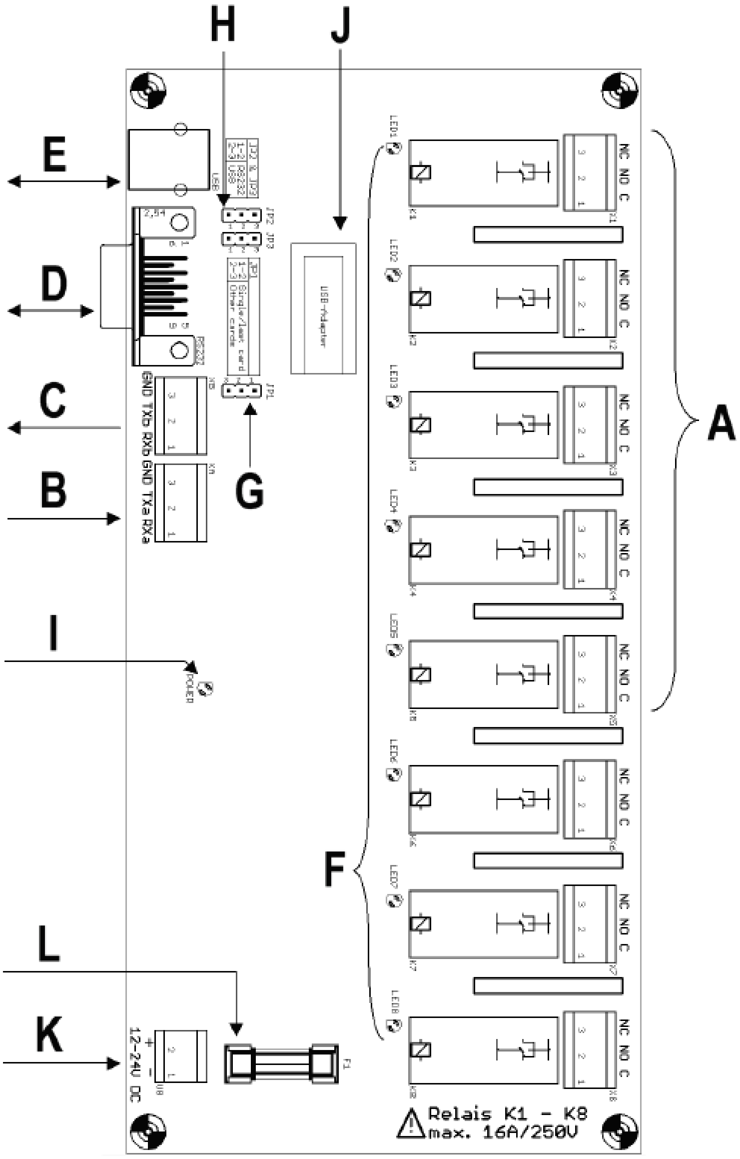

Figure 3.8: Relay card Conrad 197730 [62]. (A) Relay output, (B,C) Multiple card communication ports, (D) RS232 input, (E) USB input, (F) relay switching state LED, (G,H) Operation mode jumpers,(I) Card on/off LED,(J) RS232 to USB converter,(K) Card power source ports, (L) Card security fuse.

3.2 Software

A dedicated Labview program has been written in order to detect and save in real time the data from the sensors implemented in the system and to communicate commands to the relay card. The original program has been modified by implementing the backwash functionalities and sensors.

Labview is a graphical programming environment where the main program (VI) is made of different blocks (sub-VI), which communicate with each other through inputs and outputs, that are represented by different coloured lines, basing on the type of data being transferred.

The main VI is then converted in a user friendly interface (front panel), which is able to show the desired values acquired in the main VI and then to choose different operation modes and parameters through switching buttons or keyboard inputs. Furthermore, once the VI is optimally designed, it is possible to convert it into an executable program, which would show only the main front panel and that could be run easily in the future by not expert users.

In addition to Labview, two auxiliary programs are used: the first one is the charge controller built in programs which allows to monitor the filtration pump current and voltage at any given time, while the second one is the factory software associated to the SAS, through which it is possible to set the unit outputs as constant values or as solar days.

3.2.1 Front panel interface

As mentioned before the front panel interface shows in a clear and organized way the values of every sensor with a refresh rate within 1.5 and 2 seconds.

Fig. 3.9 shows the schematics of the system and the values of the sensors associated to every component; the yellow lines represent the electrical connections, while the blue and red lines symbolize respectively the filtration and the backwash legs. Furthermore, in the top left corner it is possible to start, stop and save the program, while on the center top, one can select the different BW modes and their associated parameters (explained in detail in sec 3.2.4)

The portion of the front panel in Fig. 3.10 shows the data processing results and time dependent trends obtained in the main VI. These data are illustrated both through real time plots on the top part and with a summarizing table on the front panel bottom.

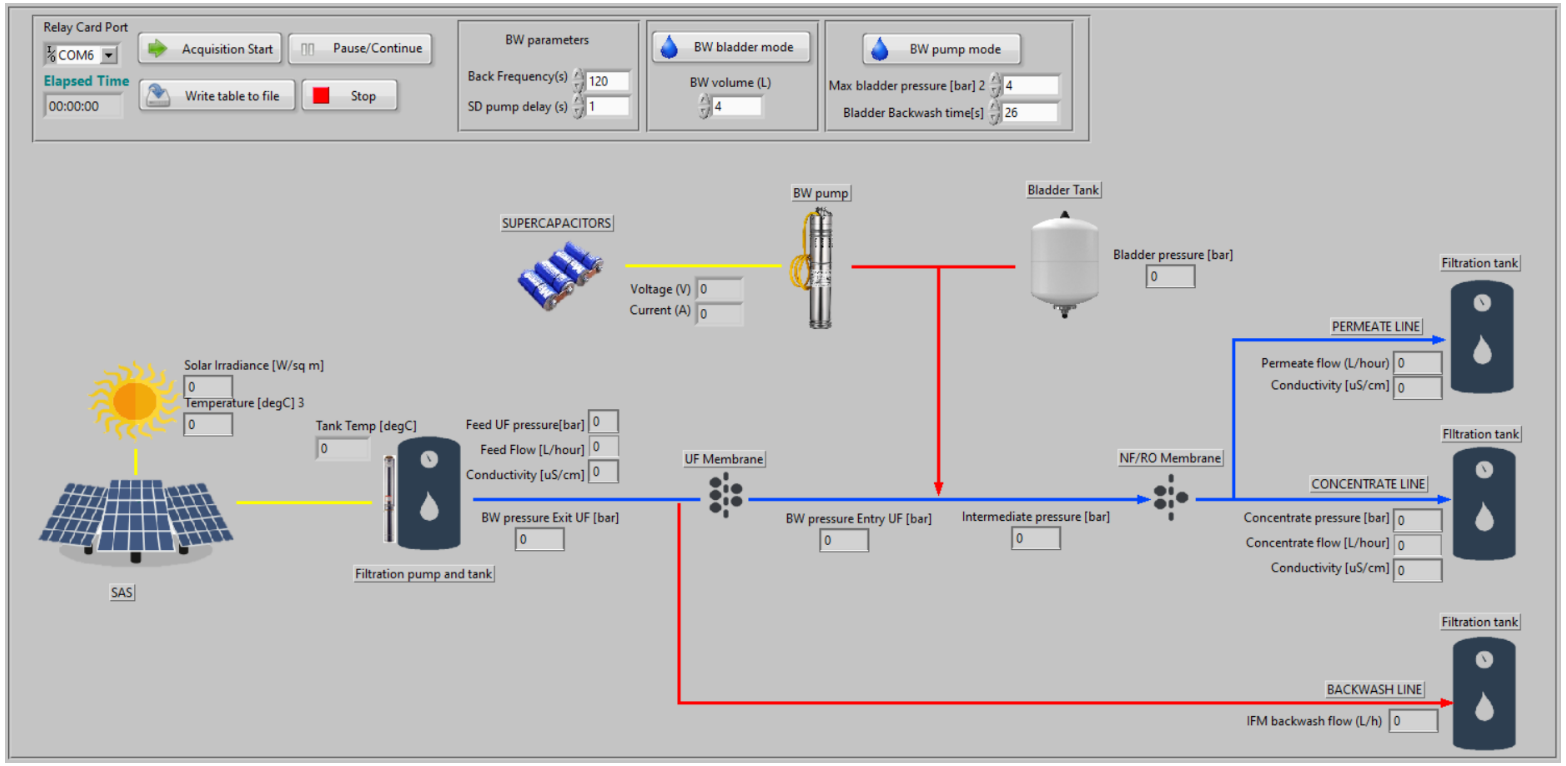

Relay Card Port: COM6

Elapsed Time: 00:00:00

Back Frequency(s) 120

SD pump delay (s) 1

BW volume (L) 4

Max bladder pressure [bar] 2 4

Bladder Backwash time[s] 26

Voltage (V) 0

Current (A) 0

Bladder pressure [bar] 0

Solar Irradiance [W/sq m] 0

Temperature [degC] 3 0

Tank Temp [degC] 0

Feed UF pressure[bar] 0

Feed Flow [L/hour] 0

Conductivity [uS/cm] 0

BW pressure Exit UF [bar] 0

BW pressure Entry UF [bar] 0

Intermediate pressure [bar] 0

Permeate flow (L/hour) 0

Conductivity [uS/cm] 0

Concentrate pressure [bar] 0

Concentrate flow [L/hour] 0

Conductivity [uS/cm] 0

IFM backwash flow (L/h) 0

Figure 3.9: Main front panel: system schematics and sensors.

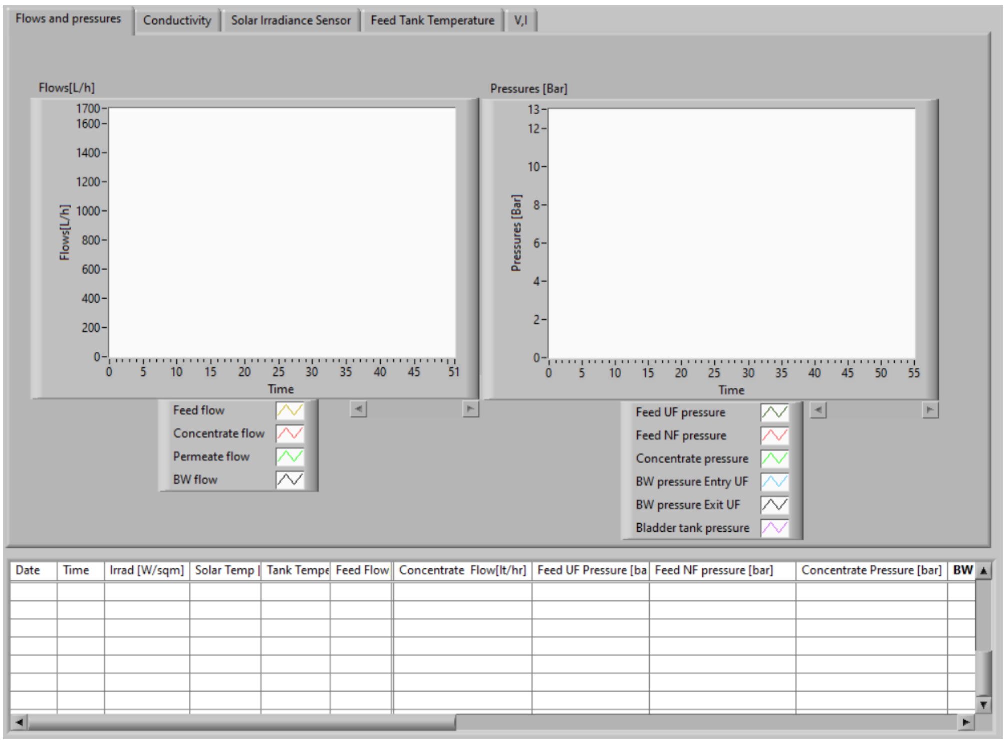

Figure 3.10: Main front panel: plots and tables.

3.2.2 Data acquisition loop

The data acquisition "while" loop (Fig. 3.11) is the section within the main VI that allows the constant communications between sensors and PC.

The BW sensors implementation is indicated by the red rectangle where the several signals are acquired by the "DAQ assistant subVI", which communicates with the data acquisition card. The data are then stored in a cluster which will be sent and processed by the following VI section.

The area not included in the rectangle contains the permeation sensors acquisition blocks which utilize a secondary group of subVIs called "DAQmx".

The "while" loop is easily paused and stopped through two dedicated buttons that also appear in the front main panel.

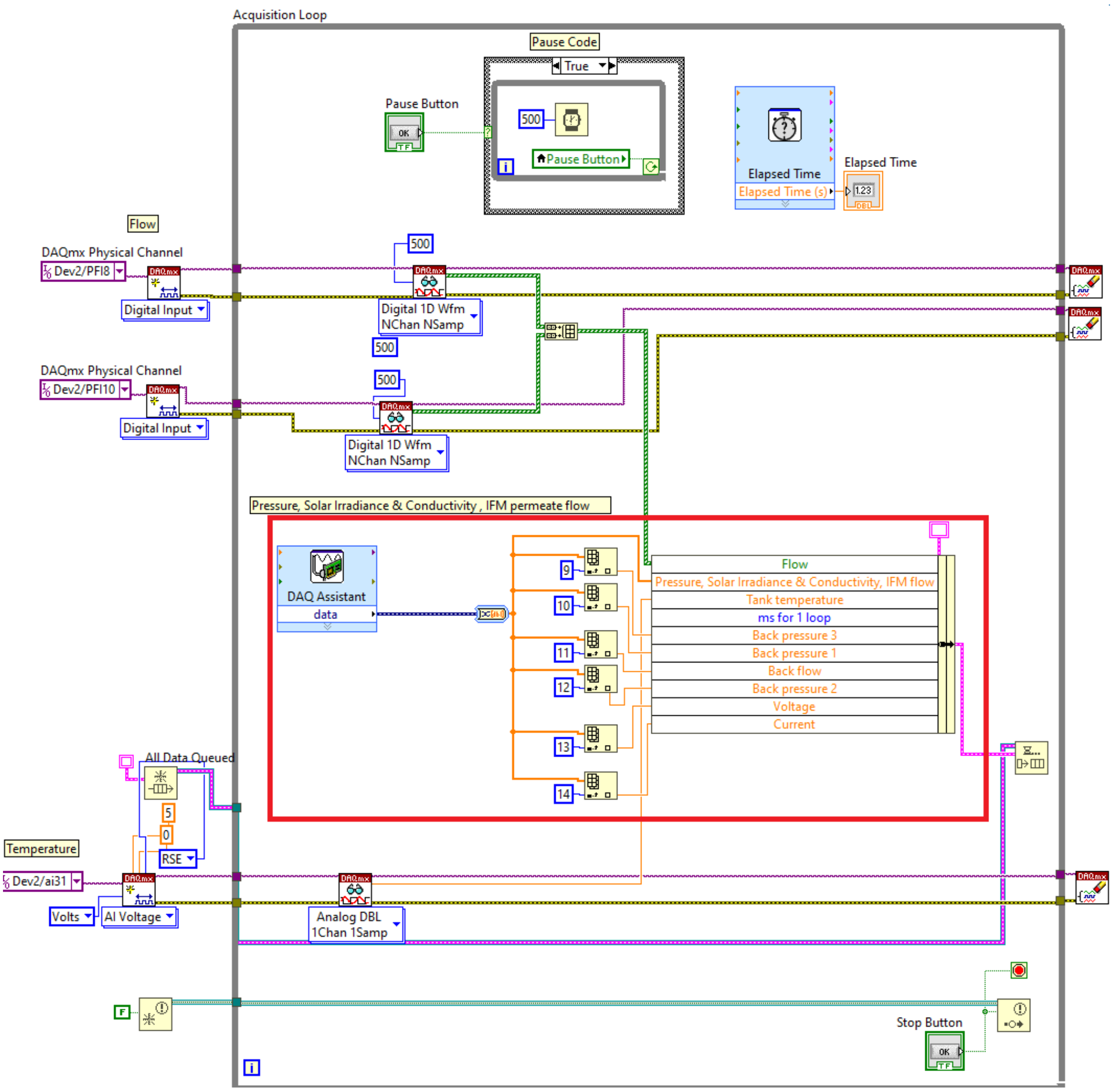

Figure 3.11: Data acquisition loop.

3.2.3 Data processing loop

The data previously acquired are then processed by a second dedicated "while" loop (Fig. 3.15). The raw signals are extracted from the storing cluster and connected as inputs to the dedicated calibration subVIs.
Concerning the BW sensors, the respective calibration subVI are contained in the red rectangles in Fig. 3.15. These blocks convert the received signal in the required quantity through the calibration formulas obtained in section 3.1.1. Each calibration subVi is shown in Fig.3.12, Fig. 3.13 and Fig. 3.14.
Every calibrated quantity is then sent to the respective plot subVIs and to the real time table processing on the bottom part of the loop.

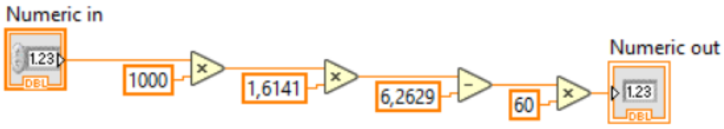

Figure 3.12: Flow sensor calibration subVI.

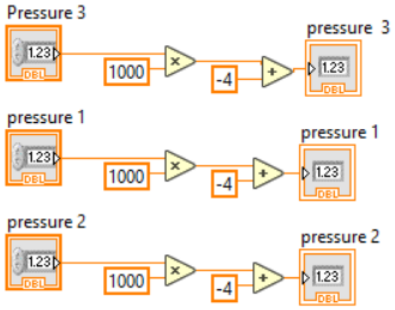

Figure 3.13: Pressure sensors calibration subVI.

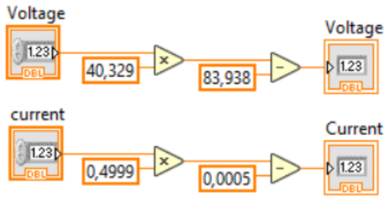

Figure 3.14: Voltage and current sensors calibration subVI.

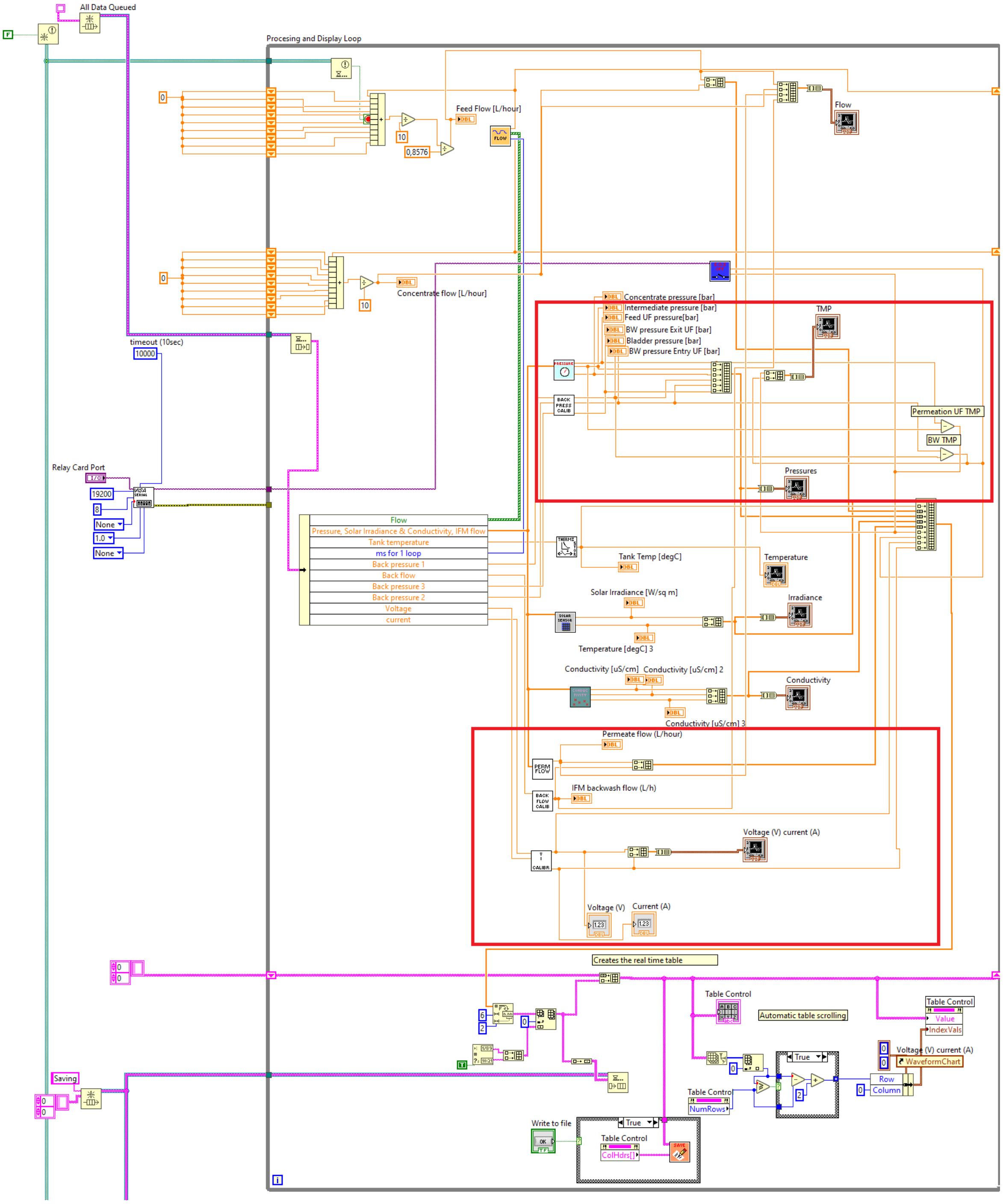

Figure 3.15: Data processing loop.

3.2.4 Backwash implementation

Depending on the type of backwash setup, the instructions given to the relay card in order to control the experiments are different; therefore, two different BW implementations have been developed: one for the BW pump mode and one for the BW Bladder tank mode (Fig. 3.16). They are both enclosed in a "if" structure that allows the programs to run only if the corresponding activation button on the main front panel is pressed.

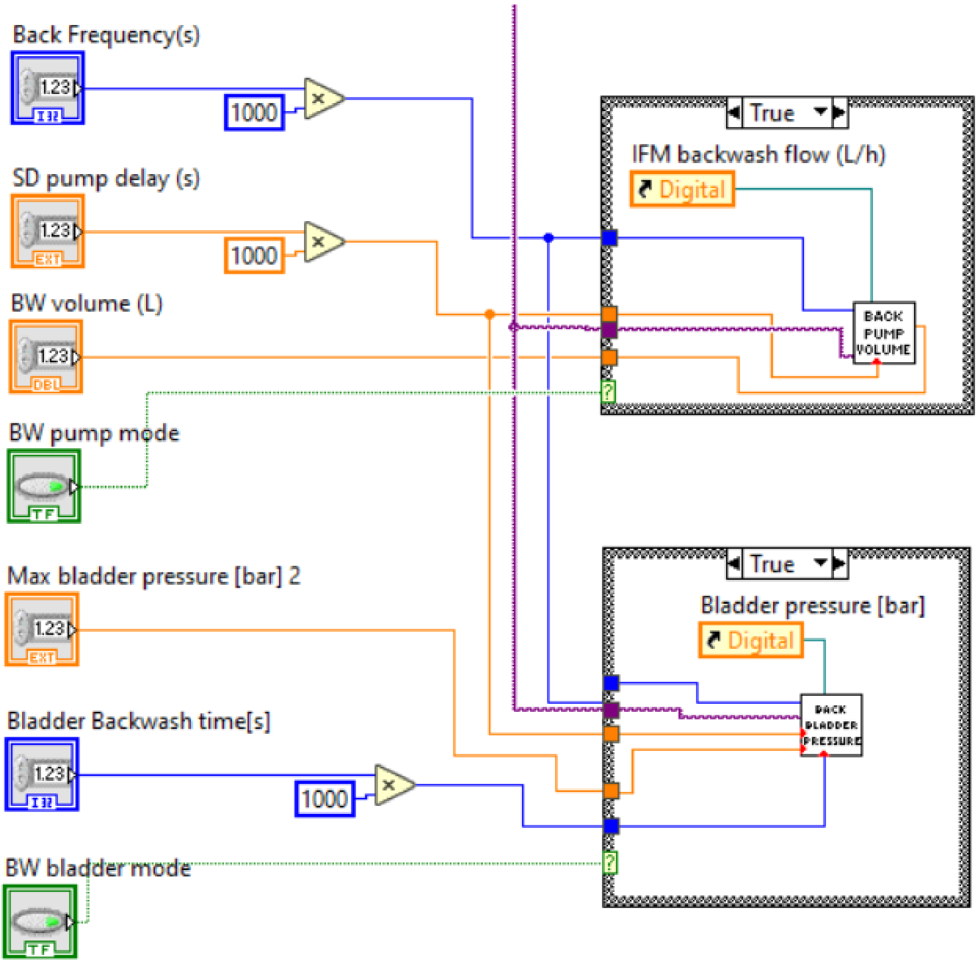

Figure 3.16: Two different backwash implementations: pump and bladder modes.

Each command to the relay card is given through a dedicated subVI illustrated in Fig. 3.17. Three numbers are given as inputs: the first one represents the action that the specific relay must perform (e.g. "6" stands for switch on and "7" for switch off), the second indicates the board address (value equal to "0" if the system utilizes a single configuration card) and finally the third one represents the single or multiple relays that the user wants to interact with in binary code.

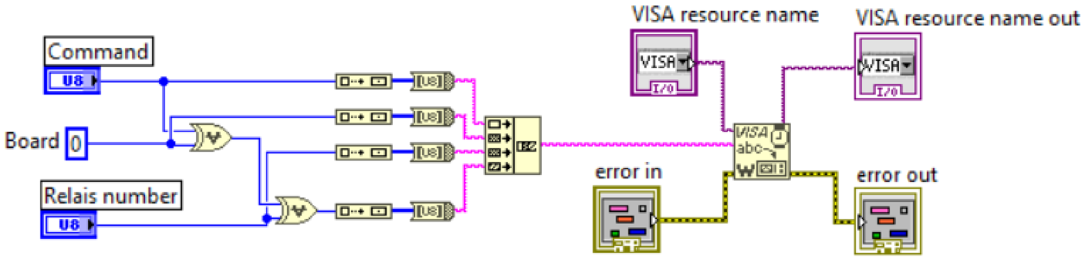

Figure 3.17: Relay card instructions subVI

Bladder tank mode

The bladder tank backwash mode is illustrated in Fig. 3.18. The entire program is enclosed in a "for" cycle for a total of 5 repetitions.
Many temporally consecutive stages characterize each cycle. In the first part the bladder tank valve is opened so that the water is allowed to flow and to be stored; the valve is then closed when the bladder tank pressure reaches a specific value set in the front main panel (in this case 4 bar). The program then waits for the BW frequency time (e.g. 30 min), then shuts down the filtration pump and finally (with a delay selectable from the main front panel, which reduces the pump mechanical stresses) it opens the BW filtration solenoidal valves, closing also the filtration one. In this way the bladder tank water is free to flow in the backwash direction for a duration of 26 s (experimentally calculated time needed to completely evacuate the tank), before starting the cycle again.

Pump mode

The pump backwash mode illustrated in Fig. 3.19 has been designed with a similar structure compared to the bladder tank counterpart. In the first part the system waits for the BW frequency (selectable in the front main panel) and then shuts down the filtration pump. The membrane backwash is then started, by activating the BW pump and by closing the filtration valve and by opening the backwash one. On the opposite of the bladder tank program, the BW duration is not set to a fixed value; indeed the user can select the desired BW water to utilize from the main front panel, so that the program can perform a real time BW flow integration, until the specified volume is reached. The BW pump is then shut down before starting the cycle again.

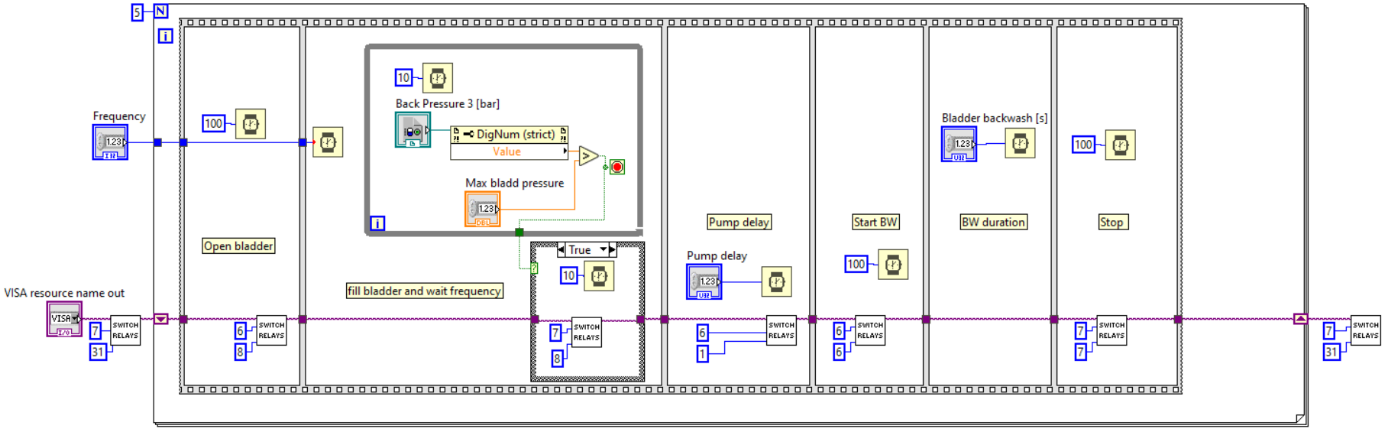

Figure 3.18: Bladder tank backwash mode.

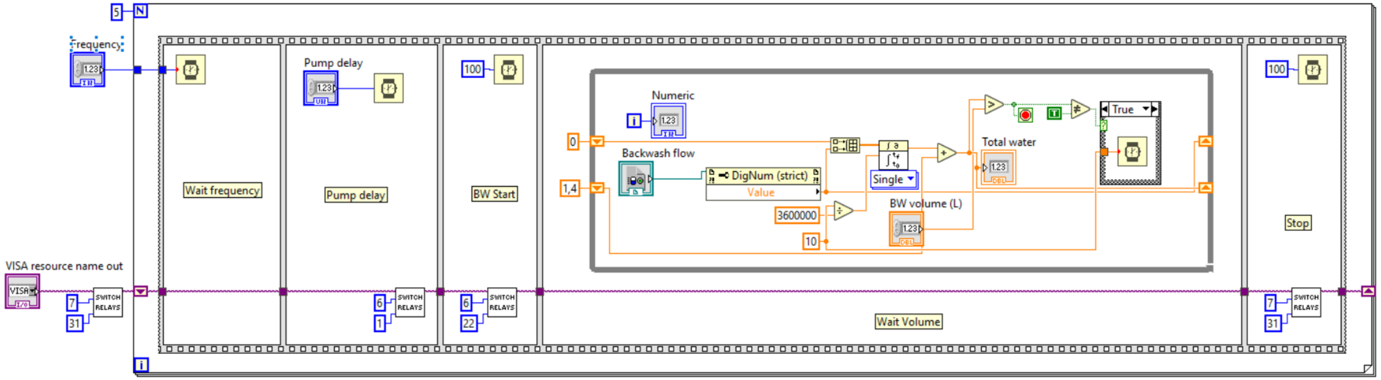

Figure 3.19: Pump backwash mode.

3.3 Experimental Protocol

The testing of the two backwash setups is meant to allow a comparison between the cleaning effectiveness and energy consumption of the two systems. In order to do so, both the configurations use the same amount of backwash water (4L) during the cleaning cycles; this value has been chosen since it is the maximum amount of water stored by the bladder tank at a pressure of $p_{bladder\_water\_side}$ =4 bar, which is the maximum pressure that does not cause an exceeding in the maximum UF membrane TMP during the BW phase. Furthermore, the filtration pump has been powered with a constant solar irradiation of 1000 W/m^2 in both cases, which is translated through the SAS built-in Sandia model into a fixed imposed voltage of 185 V. The number of cleaning cycle has been set to 5 in order to highlight the system behaviour over time. The only variable from one experiment to the other is represented by the BW frequencies, which range from 15 to 120 min.

This is the summary of the experimental parameters:

- BW water utilized: 4 L;
- Bladder tank: $p_{bladder\_water\_side}$=4 bar;
- Number of BW cycles: 5;
- Feed water salt concentration: 5 g/L;
- Feed water bentonite concentration: 500 mg/L;
- SI: 1000 W/m2 with $V_{filtration\_pump}$=185 V;
- SCs initial state of charge: completely charged (177 V);
- BW frequencies: 15, 30, 45, 60, 90, 120 min.

3.3.1 Performance indicators

UF trans-membrane pressure (TMP)

The UF TMP will be used in the results section as a fouling indicator. It represents the difference between the pressure at the entrance (feed) and at the exit of the membrane.

$$TMP_{UF}(bar) = p_{UF\_feed} - p_{UF\_exit} \tag{3.1}$$

The more material accumulates on the membrane, the higher the pressure drop across its ends, which is indicated by higher TMP values.

Total specific energy consumption (TSEC)

The energy performance of the system will be measured through the TSEC which represents the amount of energy used by the system per unit of RO permeate water.

$$TSEC(kWh/m^3) = \frac{E_{filtration\_pump} + E_{BW}}{Water_{permeation} - Water_{BW}} \tag{3.2}$$

Where the BW energy E_{BW} depends on the type of set up and it is calculated in section 4.1. This indicator therefore takes into account the total energy required by the system, composed by the filtration pump energy and the backwash cycles energy, and the total amount of drinkable water produced with that energy; it also considers the backwash water lost during the cleaning procedure.
It is important to notice that the energy required by the mixing pump is not taken into account, since it would not be included in a real application of the system.

TMP reversibility

The TMP reversibility is an indicator that gives information about the cleaning effectiveness of a backwash cycle. It is represented by the normalized difference between the TMP at the beginning of a cycle and the TMP at the beginning of the experiment (TMP_0).

$$TMP_{rev(i)}(\%) = \frac{TMP_{(i)} - TMP_0}{TMP_0} * 100 \tag{3.3}$$

This indicators is able to quantify what percentage of the initial TMP has been restored after a cleaning cycle; TMP_{rev}= 100% will represent a complete TMP recovery.

Chapter 4

Experimental results and discussion

4.1 BW cycle energy consumption

The testing of the two backwashing setups has allowed to calculate the energy required for each backwash cycle.

Bladder

The energy consumed by the bladder tank is concentrated in the filling phase, when 4 liters of water are stored at a pressure of 4 bar. In order to calculate the energy required for the water storing, a comparison between the system with and without filling phase has been performed.

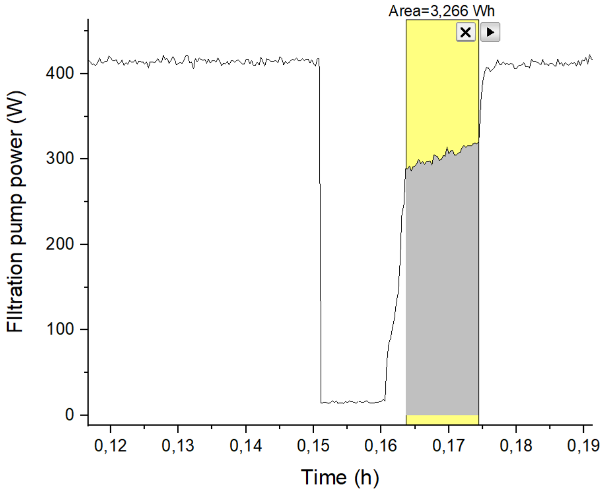

Figure 4.1: System energy consumption during the bladder tank filling phase.

The integrated area shown in Fig.4.1 represents the difference between the two operating modes and therefore the single cycle backwash energy consumption (3.266 Wh). The total energy required for a full experiments made of 5 backwash cycles will be 16.33 Wh.

BW pump

Differently from the bladder tank case, the energy required from the BW pump is made of two terms.

The first one is represented by the energy consumed in order to produce the 4 liters of water required for the backwash procedure. The water is extracted from the system after being filtrated by the UF membrane under normal steady operating conditions. The UF permeate flow has been plotted and compared to the filtration pump power consumption. The integrated area corresponding to a 4 liters water filtration has been highlighted (Fig.4.2) and transposed over the power consumption curve (Fig. 4.3), allowing the calculation of the energy required for the water production (3.77 Wh).

The second term is due to the actual electrical energy consumed by the BW pump during the BW phase. A current of 12 A at 40 V is requested by the pump for the total duration of the cleaning phase (12 s). The pump therefore utilizes 1,6 Wh per cycle. Considering a converter efficiency of around 85% the total energy demand increases to 1.88 Wh.

Therefore the sum of the two terms leads to a total energy consumption per experiment of 28.26 Wh.

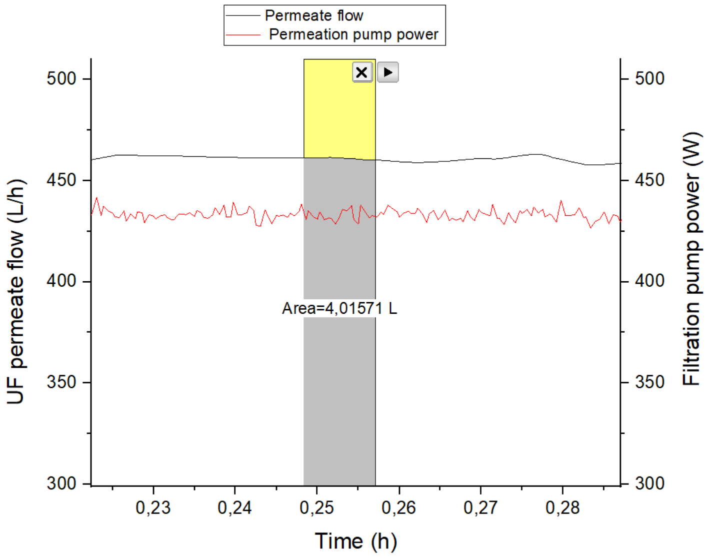

Figure 4.2: UF filtration flow and filtration pump power consumption over time (permeated liters highlighted).

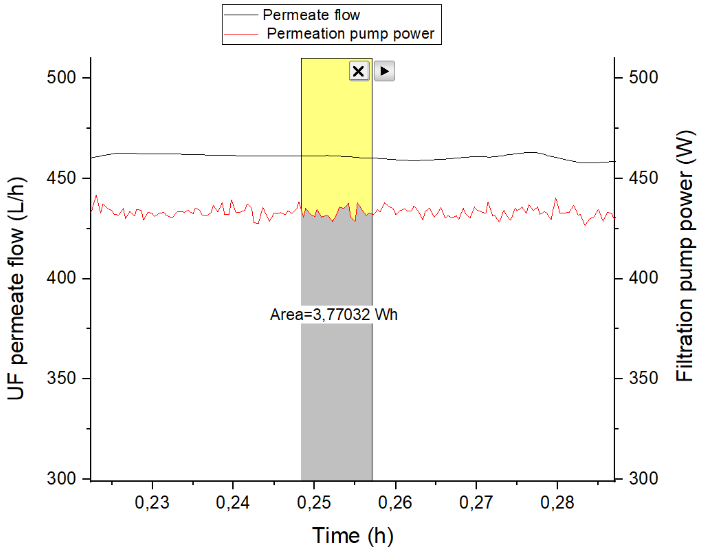

Figure 4.3: UF filtration flow and filtration pump power consumption over time (energy consumption highlighted).

4.2 Bentonite as fouling agent

The addition of bentonite with a concentration of 500 mg/L to the feed water has demonstrated to be a valid fouling simulation method. Indeed, over time, the UF membrane has shown a noticeable TMP increase illustrated in Fig. 4.4. The filtration pump adjusts to this pressure drop by increasing the power required from the SAS, resulting into a rising in the overall system energy consumption (Fig. 4.5). Since the RO permeation flow stays constant, the final result is a decrease in SEC and therefore in the system performance.

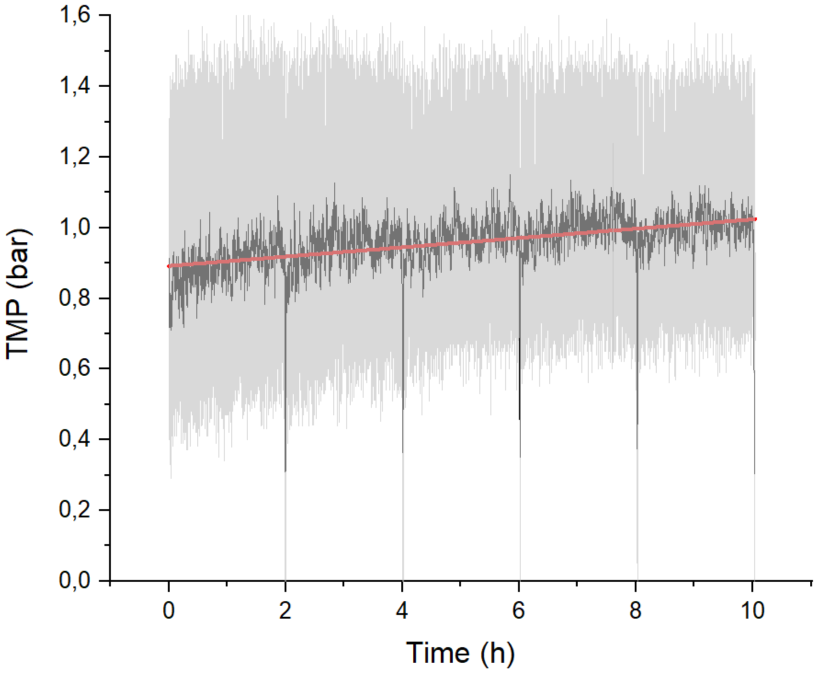

Figure 4.4: UF TMP (gray), UF TMP moving average (black), UF TMP linear fit (red) as functions of time.

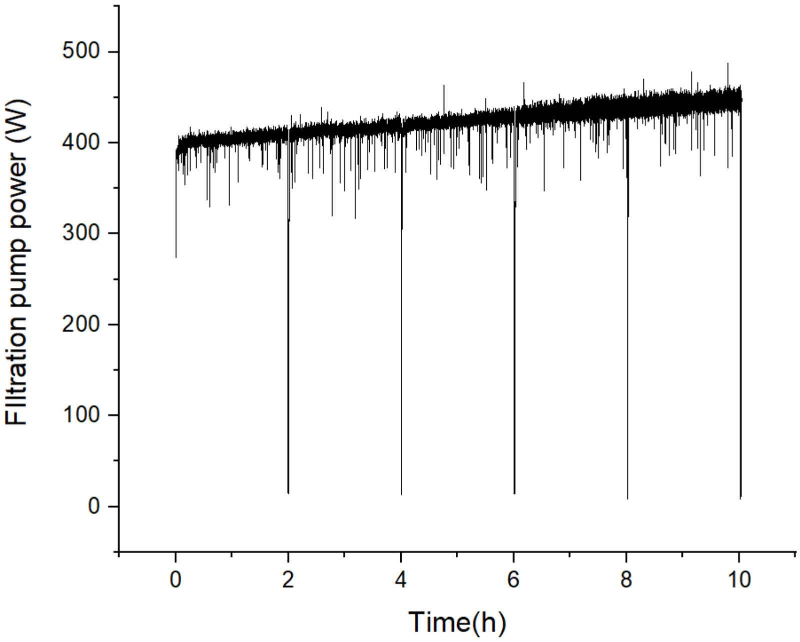

Figure 4.5: Filtration pump power consumption over time.

4.3 UF TMP as a function of cleaning frequency

As already mentioned in section 3.3 the two setups have been tested with different BW frequencies in order to monitor the TMP increase over time.

4.3.1 Bladder tank

The bladder tank setup results are illustrated in Fig.4.6. As it is possible to notice, no significant TMP increase can be highlighted for backwash frequencies ranging from 15 to 45 min. On the other hand, for values equal or higher than 60 min it is possible to notice a growing trend in TMP, which reaches the maximum slope for 120 min.

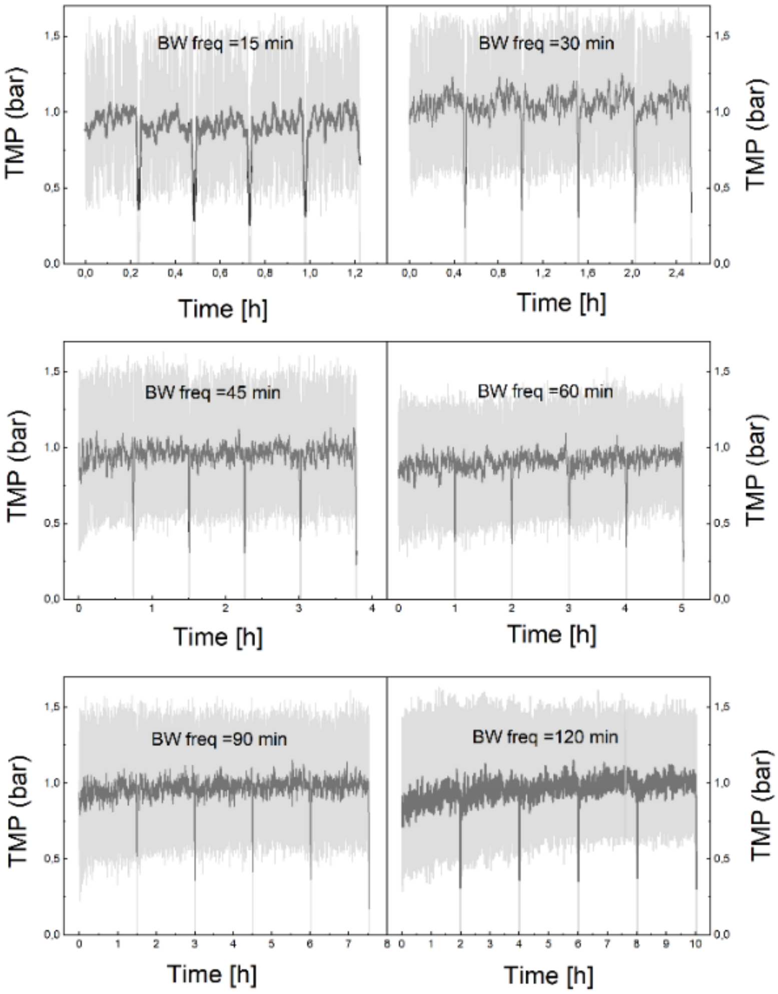

Figure 4.6: UF TMP (light gray) and corresponding moving average (black) as a function of time for different BW frequencies for the bladder tank setup.

The results therefore show that, when the membrane is subjected to frequent cleaning (up to 45 min), the bentonite has no time to accumulate inside the membrane, causing a negligible increase in TMP. On the other hand, for less frequent cleaning, the backwash cycles do not menage to completely remove the significant amount of bentonite that is able to build up on the membrane surface. This mechanism causes an increase in TMP over time, which translates into an overall increase in the filtration pump power consumption (Fig. 4.5).

4.3.2 Backwash pump

The backwash pump results (Fig.4.7) are similar to the ones of the previous configurations in terms of both TMP trend slopes and absolute values reached. The only exception is represented by the 120 min frequency experiment, where no significant TMP increase over time can be highlighted. This behaviour is in strong contrast with the results shown in the other experiments. The reasons must be still completely understood and they are probably to be found in the following mechanisms:

- **Bentonite coagulation**
  The bentonite-bentonite and bentonite-salt interactions could lead to the formation of coagulated particles in the solution. The bigger size of these agglomerations could lead to a lower fouling cake resistance and therefore to a lower detected UF TMP.

- **Bentonite concentration reduction**
  The amount of suspended bentonite particle could decrease over time for different reasons. The foulant could deposit on the bottom of the feed tank and not be reintroduced in the suspension by the mixing pump; the material could also adhere on the walls of the feed tank or on the inner walls of the system pipes.

- **Irreversible fouling**
  The pore scale fouling on the membrane surface could play a role in the reduction of the amount of bentonite suspended in the solution. For example a possible dendrite formation on the spacing between pores (Fig. 2.11) could lead to the accumulation of inactive material inside the membrane.

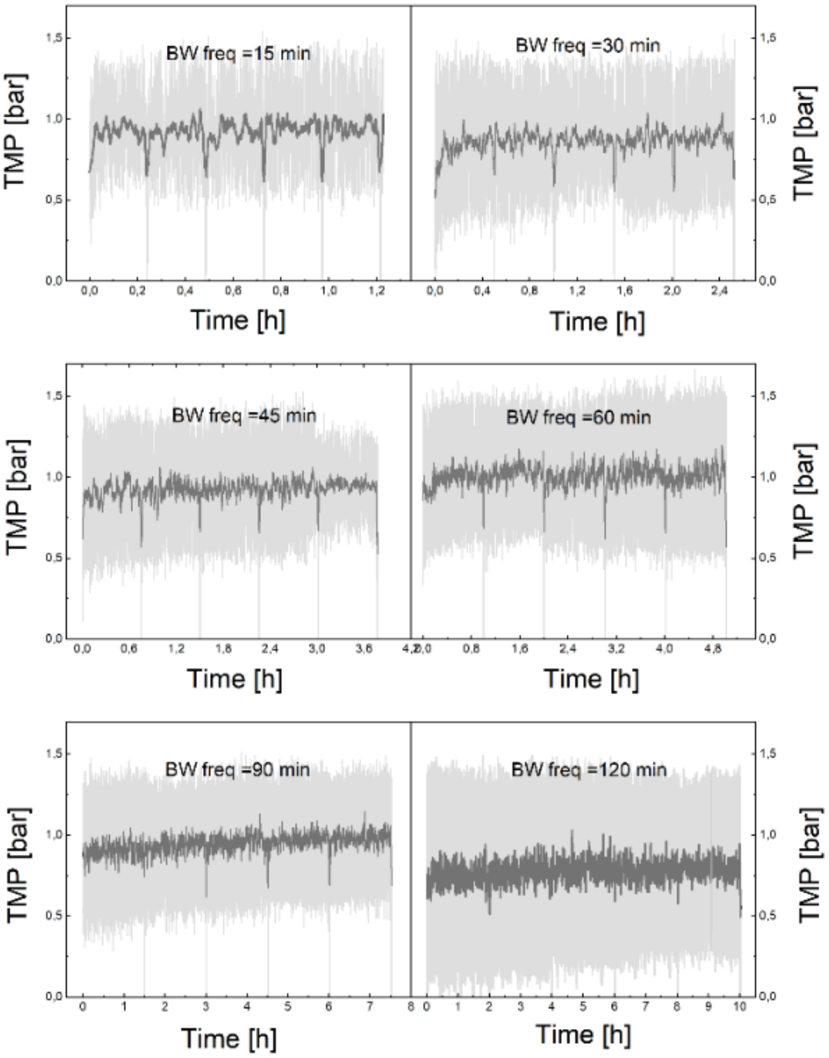

Figure 4.7: UF TMP (light gray) and corresponding moving average (black) as a function of time for different BW frequencies for the BW pump setup.

4.4 Total specific energy consumption

As already mentioned, the energy consumption of the two setups will be compared using the total specific energy consumption (TSEC).

4.4.1 Bladder tank

The bladder tank setup TSEC for different BW frequencies is shown in Fig.4.8. As it is possible to notice the total specific energy consumption decreases with less frequent cleaning; in particular it plateaus for BW frequencies longer than 30 minutes.

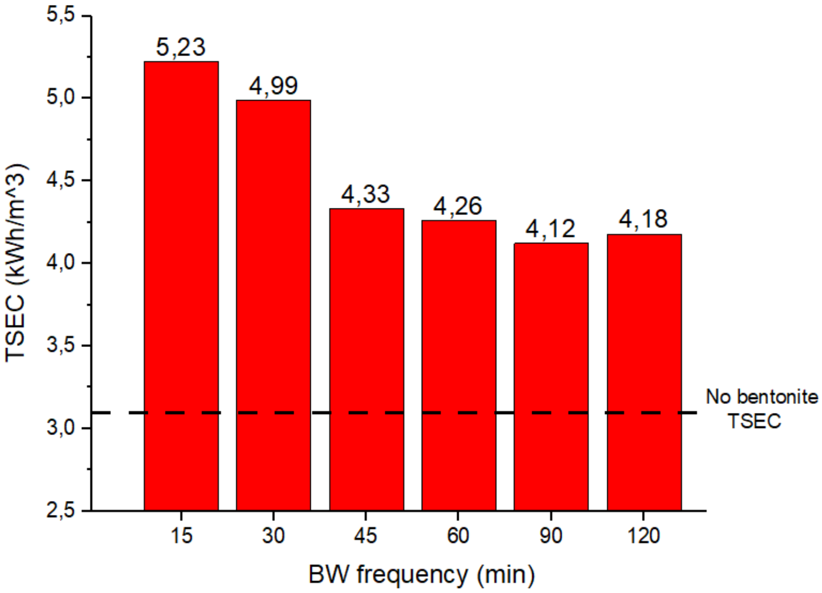

Figure 4.8: TSEC as a funtion of backwash frequencies for the bladder tank setup.

The optimal TSEC should be a trade off between the additional energy required for the BW cycles, which are necessary to clean the membrane, and the reduction in the energy utilized by the filtration pump due to previously mentioned cleaning. For shorter frequencies, the increase in energy utilization due to the frequent backwashing of the membrane is not compensated by the consequent reduction in filtration energy utilization. On the other hand, for longer frequencies (from 45 to 120 min), the additional energy required by the cleaning cycles is justified by a decrease in filtration power consumption, which brings to a lower TSEC. Ideally, for even longer frequencies, the TSEC trend could start increasing again since the bentonite fouling would cause an even higher filtration energy consumption; in that case, the increase of energy due to a more frequent cleaning of the membrane could possibly bring to a higher decrease in filtration power utilization, resulting in an overall convenient procedure.

It is also possible to notice that the introduction of bentonite and of a backwash procedure causes a significant increase in TSEC compared to the reference ideal case with no fouling agent and no UF cleaning (around 3.1 kWh/m^3).

4.4.2 Backwash pump

The results of the BW pump setup (Fig.4.9) are very similar to the ones achieved by the previous configuration. In particular the TSEC shows the same trend and similar absolute values. For the same reasons already illustrated in section 4.3, the only exception is the experiment corresponding to a cleaning frequency of 120 minutes.

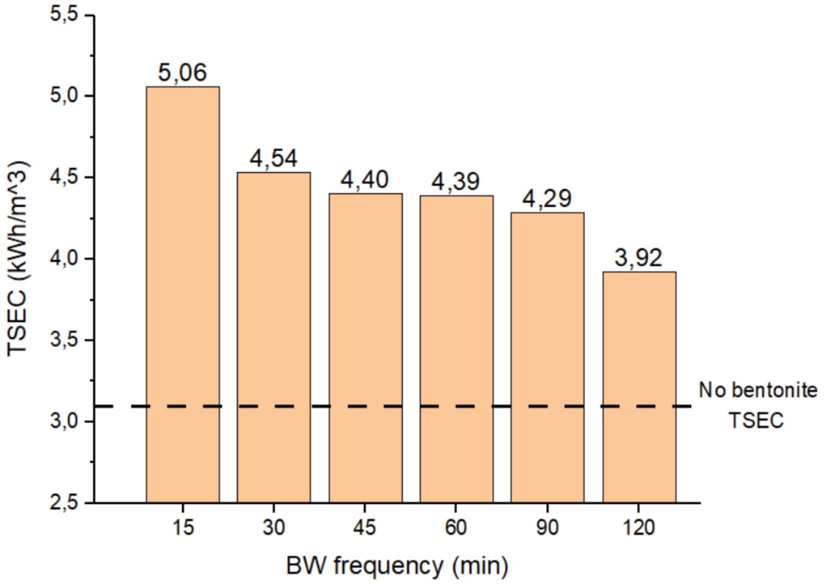

Figure 4.9: TSEC as a funtion of backwash frequencies for the BW pump setup.

4.5 TMP reversibility

As already mentioned, the TMP reversibility is an indicator which gives information about the cleaning effectiveness of a backwash cycle. The expected trend would be that shorter backwash frequencies would be able to effectively clean the membrane, restoring the initial TMP after the backwash procedure, therefore being characterized by TMP reversibility values close to 100%. The opposite behaviour could be expected for longer frequencies, where the cleaning cycles would not be able to remove the large amount of accumulated bentonite on the membrane, causing TMP reversibility values lower than 100%. The results for both the bladder tank (Fig.4.10) and BW pump (Fig.4.7) do not show any noticeable trend; indeed, even if more fouling material is physically removed from the membrane surface for more frequent cleaning, this does not necessarily translate into higher TMP reversibility values.

This not direct relation between amount of fouling agent removed from the membrane and TMP restoring is very interesting and requires further investigation in the future. The possible factors than influence this relation are to be found in the already mentioned coagulation or deposition of the bentonite particles and in the irreversible phenomena that occur on the membrane surface. Particularly interesting would be the fouling cake formation, detachment and redeposition dynamics.

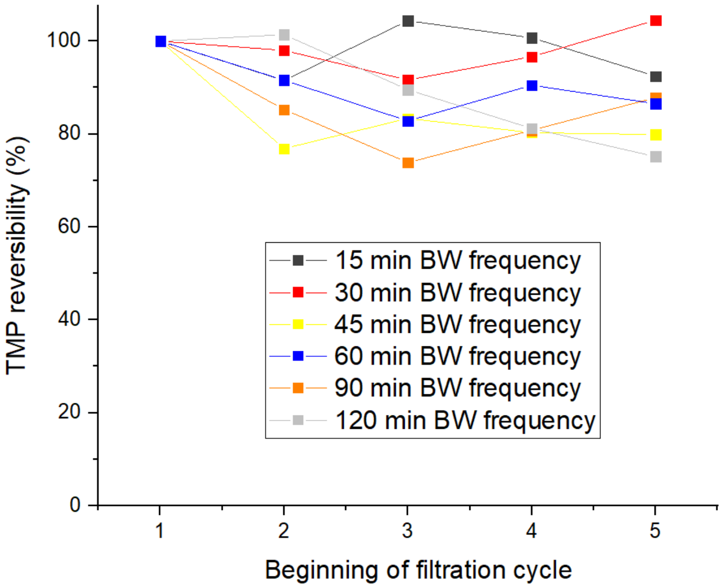

Figure 4.10: TMP reversibility over filtration cycles for different BW frequencies for the Bladder tank setup.

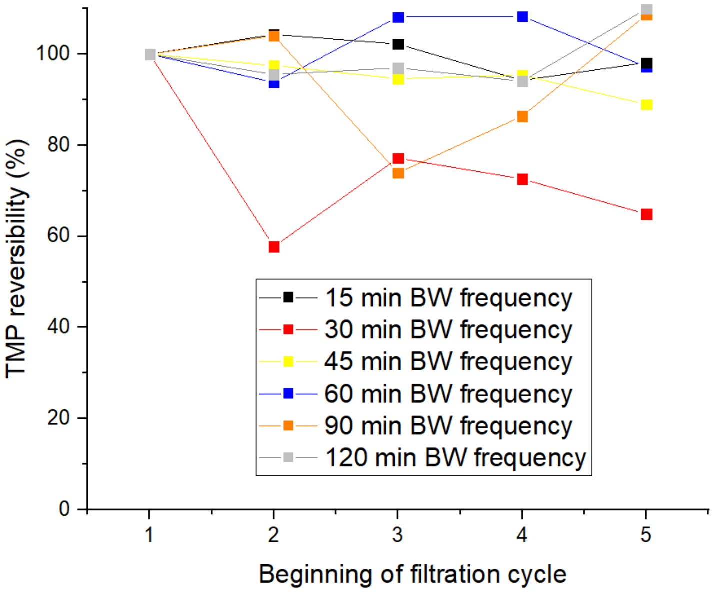

Figure 4.11: TMP reversibility over filtration cycles for different BW frequencies for the BW pump setup,

4.6 Discussion

4.6.1 Choice of the optimal BW frequency

The results show that in general it is possible to affirm that three main factors influence the decision of the optimal BW frequency:

- The TSEC plateaus for BW frequencies longer than 30 minutes;
- More frequent BW cycles remove more fouling agent from the membrane even if it does not directly imply a TMP reduction;
- The TMP increase is more noticeable for BW frequencies longer than 45 minutes.

The choice of the optimal BW frequency is strongly influenced by the usage case. Considering this work application, a backwash frequency of 90 minutes has been chosen as set value for future analysis. Indeed the two systems will be studied under real solar days conditions: in that case the amount of bentonite removed from the membrane is not a key factor, instead it is very important to be able to induce a noticeable TMP increase in order to allow a good fouling simulation, keeping the TSEC as low as possible.
On the contrary other kinds of applications are interested in keeping the membrane as clean as possible, in order to maintain a high product quality (e.g. pharmaceutical filtration systems); these kind of setups will strongly benefit from more frequent membrane

cleaning.
Another kind of application that would benefit from shorter BW frequencies is the filtration of highly polluted water. Indeed in this case a big amount of fouling material will deposit on the membrane causing a faster fouling rate compared to this work case study, requiring a more frequent cleaning procedure.

4.6.2 Choice of the optimal BW configuration

As showed by the results, the bladder tank backwash cycle requires lower energy compared to the BW pump one. Even considering this difference, the two BW configurations show very similar TSEC trends. Therefore it is not possible to choose a cleaning configuration basing on the overall system energy consumption. Similarly to the optimal BW frequency, the choice of the optimal configuration will depend on the type of application.
Concerning this work, the bladder tank setups is the preferable choice: this filtration system is indeed developed for a possible real field application in the sub-Saharan region. Then, the cost, the lack of high voltage components and the overall sturdiness of the bladder tank setup, become the crucial elements in the cleaning system selection.

Chapter 5

Conclusion

In this work, two backwash setups have been successfully implemented into a PV-powered ultrafiltration and reverse osmosis filtration system. A dedicated labview program has been written in order to control the additional cleaning operating modes. Bentonite has proven to be a suitable fouling agent, since its insertion in the DI water and salt solution, showed, as desired, a noticeable UF trans-membrane pressure (TMP) increase. The two systems have been tested over time, with different cleaning frequencies. The results are very similar for the two setups. In particular they show that the TMP increase is noticeable only for cleaning frequencies longer than 45 minutes, meaning that the fouling agent is accumulating on the membrane surface for those values. The total specific energy consumption (TSEC) of the system, which is the result of the trade off between the additional energy required for backwashing and the energy saved due to the cleanliness of the membrane, plateaus to the minimum value for cleaning frequencies longer than 30 min. Finally, no noticeable trend in the TMP reversibility data show that a more in depth pore-scale fouling analysis must be performed. The two systems have presented similar results in both TMP and TSEC terms, shifting, in this work case, the decision of the optimal configuration on external factors like cost and general sturdiness, where the bladder tank is the best option. The optimal BW frequency for this work future application will be 90 min, since it will allow to reach a noticeable TMP increase in the experiments, with a low total specific energy consumption.

Since the backwash setups are successfully implemented, the opportunity for future research is very broad. For example it would be interesting to test these systems with real solar days irradiances, in order to analyse how the configurations react to sudden reduction in source power. It would be also possible to test different kind of fouling material at different concentrations, in order to compare the results with the ones achieved in this work and possibly get some insight on the different particle-particle and particle-membrane interactions. It would be also relevant to analyze how triggering the BW only when it is required (for a specific UF TMP threshold) could influence the TSEC of the system.

List of Figures

List of Tables

Bibliography

[1] "Understanding key water stewardship terms." https://ceowatermandate.org/terminology/ , Access: 2019-10-24.

[2] E. Swyngedouw, "Un water report 2012: depoliticizing water," *Development and Change*, vol. 44, no. 3, pp. 823–835, 2013.

[3] "International water menagement institute." http://www.iwmi.cgiar.org , Access: 2019-10-25.

[4] B. S. Richards, J. Shen, and A. I. Schäfer, "Water–energy nexus perspectives in the context of photovoltaic-powered decentralized water treatment systems: A tanzanian case study," *Energy Technology*, vol. 5, no. 7, pp. 1112–1123, 2017.

[5] "World energy outlook 2018." https://www.iea.org/weo2018/ , Access: 2019-10-25.

[6] I. Ouedraogo, P. Defourny, and M. Vanclooster, "Mapping the groundwater vulnerability for pollution at the pan african scale," *Science of the Total Environment*, vol. 544, pp. 939–953, 2016.

[7] "Global solar atlas." https://globalsolaratlas.info/map?c=13.271266,-44.648438,2 , Access: 2019-10-25.

[8] I. G. Wenten, "Recent development in membrane science and its industrial applications," *J Sci Technol Membrane Sci Technol*, vol. 24, no. Suppl, pp. 1010–1024, 2002.

[9] A. Fane, "Membranes for water production and wastewater reuse," *Desalination*, vol. 106, no. 1-3, pp. 1–9, 1996.

[10] M. A. El-Ghaffar and H. A. Tieama, "A review of membranes classifications, configurations, surface modifications, characteristics and its applications in water purification," *Chemical and Biomolecular Engineering*, vol. 2, no. 2, p. 57, 2017.

[11] X. Shi, G. Tal, N. P. Hankins, and V. Gitis, “Fouling and cleaning of ultrafiltration membranes: a review,” *Journal of Water Process Engineering*, vol. 1, pp. 121–138, 2014.

[12] R. W. Baker, *Membrane technology and applications*. John Wiley & Sons, 2012.

[13] R. Field, “Fundamentals of fouling,” *Membranes for water treatment*, vol. 4, pp. 1–23, 2010.

[14] D. Hughes and R. Field, “Crossflow filtration of washed and unwashed yeast suspensions at constant shear under nominally sub-critical conditions,” *Journal of membrane science*, vol. 280, no. 1-2, pp. 89–98, 2006.

[15] D. Jermann, W. Pronk, R. Kägi, M. Halbeisen, and M. Boller, “Influence of interactions between nom and particles on uf fouling mechanisms,” *Water research*, vol. 42, no. 14, pp. 3870–3878, 2008.

[16] K. Scott, *Handbook of industrial membranes*. Elsevier, 1995.

[17] Z. Cui, “Protein separation using ultrafiltrationâFIXME”an example of multi-scale complex systems,” *China Particuology*, vol. 3, no. 6, pp. 343–348, 2005.

[18] W. Yuan and A. L. Zydney, “Humic acid fouling during microfiltration,” *Journal of Membrane Science*, vol. 157, no. 1, pp. 1–12, 1999.

[19] P. Bacchin, P. Aimar, and R. W. Field, “Critical and sustainable fluxes: theory, experiments and applications,” *Journal of membrane science*, vol. 281, no. 1-2, pp. 42–69, 2006.

[20] R. W. Field, D. Wu, J. A. Howell, and B. B. Gupta, “Critical flux concept for microfiltration fouling,” *Journal of membrane science*, vol. 100, no. 3, pp. 259–272, 1995.

[21] G. Pearce and R. Field, “Development of the sustainable flux concept to provide guidelines for fouling control in uf/mf system design,” *2007 Membrane Technology Conference and Exposition Proceedings*, 01 2007.

[22] E. J. W. Verwey, J. T. G. Overbeek, and K. Van Nes, *Theory of the stability of lyophobic colloids: the interaction of sol particles having an electric double layer*. Elsevier Publishing Company, 1948.

[23] G. Trefalt and M. Borkovec, “Overview of dlvo theory,” *Laboratory of Colloid and Surface Chemistry, University of Geneva*, vol. 29, 2014.

[24] E. J. W. Verwey, "Theory of the stability of lyophobic colloids.," *The Journal of Physical Chemistry*, vol. 51, no. 3, pp. 631–636, 1947.

[25] M. Von Smoluchowski, "Mathematical theory of the kinetics of the coagulation of colloidal solutions," *Z. Phys. Chem*, vol. 92, pp. 129–168, 1917.

[26] P. Bacchin, A. Marty, P. Duru, M. Meireles, and P. Aimar, "Colloidal surface interactions and membrane fouling: Investigations at pore scale," *Advances in colloid and interface science*, vol. 164, no. 1-2, pp. 2–11, 2011.

[27] P. Bacchin, P. Aimar, and V. Sanchez, "Model for colloidal fouling of membranes," *AIChE journal*, vol. 41, no. 2, pp. 368–376, 1995.

[28] A. L. Kholodenko and J. F. Douglas, "Generalized stokes-einstein equation for spherical particle suspensions," *Phys. Rev. E*, vol. 51, pp. 1081–1090, Feb 1995.

[29] Y.-X. Yu, A.-W. Tian, and G.-H. Gao, "Prediction of collective diffusion coefficient of bovine serum albumin in aqueous electrolyte solution with hard-core two-yukawa potential," *Physical Chemistry Chemical Physics*, vol. 7, no. 12, pp. 2423–2428, 2005.

[30] C. Van den Broeck, F. Lostak, and H. Lekkerkerker, "The effect of direct interactions on brownian diffusion," *The Journal of Chemical Physics*, vol. 74, no. 3, pp. 2006–2010, 1981.

[31] P. Bacchin and P. Aimar, "Critical fouling conditions induced by colloidal surface interaction: from causes to consequences," *Desalination*, vol. 175, no. 1, pp. 21–27, 2005.

[32] P. Bacchin, P. Aimar, and V. Sanchez, "Influence of surface interaction on transfer during colloid ultrafiltration," *Journal of Membrane Science*, vol. 115, no. 1, pp. 49–63, 1996.

[33] A. E. Scheidegger, "The physics of flow through porous media," *Soil Science*, vol. 86, no. 6, p. 355, 1958.

[34] J. Lin, D. Bourrier, M. Dilhan, and P. Duru, "Particle deposition onto a microsieve," *Physics of fluids*, vol. 21, no. 7, p. 073301, 2009.

[35] N. P. De Souza and O. D. Basu, "Comparative analysis of physical cleaning operations for fouling control of hollow fiber membranes in drinking water treatment," *Journal of membrane science*, vol. 436, pp. 28–35, 2013.

[36] E. E. Systems, "Mbr - envirocube submerged ultrafiltration," 2018.

[37] W. Gao, H. Liang, J. Ma, M. Han, Z.-l. Chen, Z.-s. Han, and G.-b. Li, "Membrane fouling control in ultrafiltration technology for drinking water production: a review," *Desalination*, vol. 272, no. 1-3, pp. 1–8, 2011.

[38] P. Lipp, "State of the art in drinking water treatment by mf/uf in germanyâ-FIXME"a survey among mf/uf plants," *Water Science and Technology: Water Supply*, vol. 8, no. 4, pp. 377–381, 2008.

[39] K. N Bourgeous, J. L Darby, and G. Tchobanoglous, "Ultrafiltration of wastewater: Effects of particles, mode of operation, and backwash effectiveness," *Water research*, vol. 35, pp. 77–90, 02 2001.

[40] C. Liu, S. Caothien, J. Hayes, T. Caothuy, T. Otoyo, and T. Ogawa, "Membrane chemical cleaning: from art to science," *Pall Corporation, Port Washington, NY*, vol. 11050, 2001.

[41] N. Porcelli and S. Judd, "Chemical cleaning of potable water membranes: a review," *Separation and Purification Technology*, vol. 71, no. 2, pp. 137–143, 2010.

[42] C. Shorrock and M. Bird, "Membrane cleaning: chemically enhanced removal of deposits formed during yeast cell harvesting," *Food and Bioproducts Processing*, vol. 76, no. 1, pp. 30–38, 1998.

[43] S. Hong and M. Elimelech, "Chemical and physical aspects of natural organic matter (nom) fouling of nanofiltration membranes," *Journal of membrane science*, vol. 132, no. 2, pp. 159–181, 1997.

[44] E. M. Thurman, *Organic geochemistry of natural waters*, vol. 2. Springer Science & Business Media, 2012.

[45] L. J. Zeman and A. L. Zydney, *Microfiltration and ultrafiltration: principles and applications*. CRC Press, 2017.

[46] Y. Bessiere, C. Guigui, P. Remize, and C. Cabassud, "Coupling air-assisted backwash and rinsing steps: a new way to improve ultrafiltration process operation for inside-out hollow fibre modules," *Desalination*, vol. 240, no. 1-3, pp. 71–77, 2009.

[47] A. Massé, H. N. Thi, P. Legentilhomme, and P. Jaouen, "Dead-end and tangential ultrafiltration of natural salted water: influence of operating parameters on specific energy consumption," *Journal of membrane science*, vol. 380, no. 1-2, pp. 192–198, 2011.

[48] K. Parameshwaran, A. Fane, B. Cho, and K. Kim, "Analysis of microfiltration performance with constant flux processing of secondary effluent," *Water Research*, vol. 35, no. 18, pp. 4349–4358, 2001.

[49] P. A. Maurice, M. J. Pullin, S. E. Cabaniss, Q. Zhou, K. Namjesnik-Dejanovic, and G. R. Aiken, “A comparison of surface water natural organic matter in raw filtered water samples, xad, and reverse osmosis isolates,” *Water research*, vol. 36, no. 9, pp. 2357–2371, 2002.

[50] E. Mohora, S. Rončević, J. Agbaba, A. Tubić, M. Mitić, M. Klašnja, and B. Dalmacija, “Removal of arsenic from groundwater rich in natural organic matter (nom) by continuous electrocoagulation/flocculation (ecf),” *Separation and Purification Technology*, vol. 136, pp. 150–156, 2014.

[51] E. Akhondi, F. Wicaksana, and A. G. Fane, “Evaluation of fouling deposition, fouling reversibility and energy consumption of submerged hollow fiber membrane systems with periodic backwash,” *Journal of membrane science*, vol. 452, pp. 319–331, 2014.

[52] K. Katsoufidou, S. Yiantsios, and A. Karabelas, “Experimental study of ultrafiltration membrane fouling by sodium alginate and flux recovery by backwashing,” *Journal of Membrane Science*, vol. 300, no. 1-2, pp. 137–146, 2007.

[53] L. D. Nghiem, N. Oschmann, and A. I. Schäfer, “Fouling in greywater recycling by direct ultrafiltration,” *Desalination*, vol. 187, no. 1-3, pp. 283–290, 2006.

[54] R. Pianta, M. Boller, M.-L. Janex, A. Chappaz, B. Birou, R. Ponce, and J.-L. Walther, “Micro-and ultrafiltration of karstic spring water,” *Desalination*, vol. 117, no. 1-3, pp. 61–71, 1998.

[55] Y. Li, X. Zhang, W. Zhang, J. Wang, and C. Chen, “Effect of powdered activated carbon on immersed hollow fiber ultrafiltration membrane fouling caused by particles and natural organic matter,” *Desalination*, vol. 278, no. 1-3, pp. 443–446, 2011.

[56] P. Remize, C. Guigui, and C. Cabassud, “Evaluation of backwash efficiency, definition of remaining fouling and characterisation of its contribution in irreversible fouling: Case of drinking water production by air-assisted ultra-filtration,” *Journal of Membrane Science*, vol. 355, no. 1-2, pp. 104–111, 2010.

[57] Y. Ye, V. Chen, and P. Le-Clech, “Evolution of fouling deposition and removal on hollow fibre membrane during filtration with periodical backwash,” *Desalination*, vol. 283, pp. 198–205, 2011.

[58] G. L. Park, A. I. Schäfer, and B. S. Richards, “Renewable energy powered membrane technology: The effect of wind speed fluctuations on the performance of a wind-powered membrane system for brackish water desalination,” *Journal of Membrane Science*, vol. 370, no. 1-2, pp. 34–44, 2011.

[59] Inge, *Operator's Manual 2.1 E inge*, 2014.

[60] "Tixoton." https://www.clariant.com/de/Solutions/Products/2014/02/21/13/43/Tixoton , Access: 2019-10-03.

[61] "Sanibel 6140017." https://www.sanibel.de/profibereich/artikel-stammdaten/comfort-ausdehnungsgefasse-und-zubehor/comfort-membran-druckausdehnungsgefass-18/ , Access: 2019-10-03.

[62] C. E. B. B.V., *Operation instructions 8-Way Relay Board*, 2012.